eLife

Reviewed Preprint
v2 • November 5, 2024
Revised by authors

Reviewed Preprint
v1 • November 13, 2023

Developmental Biology

Laminin γ1-dependent basement membranes are instrumental to ensure proper olfactory placode shape, position and boundary with the brain, as well as olfactory axon development

Pénélope Tignard, Karen Pottin, Audrey Geeverding, Mohamed Doulazmi, Mélody Cabrera, Coralie Fouquet, Mathilde Liffran, Jonathan Fouchard, Marion Rosello, Shahad Albadri, Filippo Del Bene, Alain Trembleau, Marie A Breau

Sorbonne Université, Centre National de la Recherche Scientifique (CNRS UMR7622), Institut de Biologie Paris-Seine (IBPS), Developmental Biology Laboratory, Paris, France • Sorbonne Université, Centre National de la Recherche Scientifique (CNRS UMR8246), Inserm U1130, Institut de Biologie Paris Seine (IBPS), Neuroscience Paris Seine (NPS), Paris, France • Imaging Facility, Institut de Biologie Paris-Seine (IBPS), Paris, France • Sorbonne Université, Centre National de la Recherche Scientifique (CNRS UMR8256), Institut de Biologie Paris Seine (IBPS), Adaptation Biologique et Vieillissement, Paris, France • Sorbonne Université, INSERM, CNRS, Institut de la Vision, Paris, France • Institut National de la Santé et de la Recherche Médicale (INSERM), Paris, France

eLife Assessment

This **important** study describes the function of Laminin γ1-dependent basement membranes in development of the olfactory placode, including morphogenesis of the placode, boundary formation, and olfactory axonal pathfinding. The study uses elegant live imaging approaches and extensive quantitative analyses, combined with detailed mutant analyses to provide a **compelling** description of the role of Laminin in olfactory placode development. In addition to the contributions this study makes to understanding olfactory placode development, it will also be of broader interest to individuals studying extracellular matrix regulation of tissue morphogenesis, and neural development including neuronal pathfinding.

https://doi.org/10.7554/eLife.92004.2.sa4

Abstract

Despite recent progress, the complex roles played by the extracellular matrix in development and disease are still far from being fully understood. Here, we took advantage of the zebrafish *sly* mutation which affects Laminin γ1, a major component of basement membranes, to explore its role in the development of the olfactory system. Following a detailed characterisation of Laminin distribution in the developing olfactory circuit, we

analysed basement membrane integrity, olfactory placode and brain morphogenesis, and olfactory axon development in *sly* mutants, using a combination of immunochemistry, electron microscopy and quantitative live imaging of cell movements and axon behaviours. Our results point to an original and dual contribution of Laminin γ1-dependent basement membranes in organising the border between the olfactory placode and the adjacent brain: they maintain placode shape and position in the face of major brain morphogenetic movements, they establish a robust physical barrier between the two tissues while at the same time allowing the local entry of the sensory axons into the brain and their navigation towards the olfactory bulb. This work thus identifies key roles of Laminin γ1-dependent basement membranes in neuronal tissue morphogenesis and axon development *in vivo*.

Introduction

The extracellular matrix (ECM) is a network of glycoproteins which provides support to tissues by contributing to mechanical and chemical signals regulating their biology. It regulates multiple processes, including cell migration, survival/proliferation, differentiation and polarity (Walma and Yamada, 2020). In addition to the fundamental role of ECM in development and homeostasis, mutations in matrix genes lead to a variety of genetic disorders, and abnormal ECM remodelling drives disease progression in fibrosis, neurological disorders and cancer (Karamanos et al., 2021; Soleman et al., 2013; Theocharis et al., 2019; Yamada et al., 2022). ECM components are also critical factors in tissue engineering and regenerative medicine (Kaur et al., 2021; Kim et al., 2021), and thus represent valuable targets but also key players in a plethora of therapeutic applications.

The ECM can influence development and disease in many ways, and despite recent advances, the full complexity of ECM functions is far from being understood. This partly comes from the lack of tools to investigate ECM roles *in vivo*. Indeed, loss-of-function of ECM components often leads to embryonic lethal phenotypes, for instance during implantation and gastrulation in mice (see for example Miner and Yurchenco, 2004), precluding the analysis of ECM functions at later stages of development.

Laminins are major components of the basement membrane (BM), a layer of ECM lying on the basal side of epithelia, which is essential for their development and homeostasis. Laminins are crucial to initiate BM assembly (Anderson et al., 2009; Huang et al., 2003; Miner and Yurchenco, 2004; Urbano et al., 2009). They are α/β/γ heterotrimers, with Laminin 111 believed to be the predominant isoform during early development (Miner and Yurchenco, 2004). The zebrafish *sly*^{wi390} (*sleepy/lamc1*) mutation (Wiellette et al., 2004) affects Laminin γ1, present in 10 out of 18 isoforms. *sly* homozygous mutants exhibit defects in notochord, blood vessel and somite morphogenesis (Dolez et al., 2011; Odenthal et al., 1996; Parsons et al., 2002; Pollard et al., 2006; Stemple et al., 1996). Maternal or residual expression of the γ1 chain until around 12 hpf (hours-post-fertilisation) (Dolez et al., 2011; Parsons et al., 2002) likely allows *sly* mutants to develop until 48-72 hpf, thus providing an *in vivo* setting to examine later functions of this ECM component.

In this study, we took advantage of the *sly* mutant to investigate the role of Laminin γ1 in the development of the zebrafish olfactory system, which forms through the growth of the axons from the olfactory placode (OP) to the olfactory bulb in the brain (Miyasaka et al., 2007) in the context of morphogenetic movements shaping the OP and nearby tissues (Aguillon et al., 2020; Breau et al., 2017; Hauptmann and Gerster, 2000; Monnot et al., 2022; Ross et al., 1992). Laminin-rich BMs are known to surround the developing OPs and adjacent brain (Torres-Paz and Whitlock, 2014; Torres-Paz et al., 2021), but their function in the construction of the olfactory system remains uncharacterised.

Laminin stimulates neurite outgrowth for many types of neurons *in vitro* (reviewed in Powell and Kleinman, 1997). *In vivo*, in the developing nervous system, Laminin is important for neuro-epithelial morphogenesis (Bryan et al., 2016; Ivanovitch et al., 2013; Sidhaye and Norden, 2017; Tsuda et al., 2010), neuronal migration (Belvindrah et al., 2007; Chen et al., 2009; Grant and Moens, 2010; Sittaramane et al., 2009) and multiple aspects of axonal development including axon emergence (Moore et al., 2022; Randlett et al., 2011; Wolman et al., 2008), growth, and pathfinding (Bonner and O'Connor, 2001; Chen et al., 2009; García-Alonso et al., 1996; Karlstrom et al., 1996; Paulus and Halloran, 2006).

Here, we provide a detailed characterisation of Laminin expression during the construction of the zebrafish olfactory system, in fixed and live embryos. We then use the *sly* mutant, combined with live imaging to quantify cell/tissue movements and axon behaviours, to investigate Laminin γ1 functions in neuronal tissue morphogenesis and axon development *in vivo*. We found that Laminin γ1-dependent BMs are instrumental to maintain proper OP morphology and position, to define the boundary between the OP and the brain and to allow the growth and pathfinding of the olfactory axons towards the olfactory bulb.

Results

The developing OP and brain tissues are surrounded by Laminin-containing BMs

We first analysed Laminin distribution during early OP morphogenesis. It has been proposed that the zebrafish OP contains a transient population of pioneer neurons in the ventro-medial region of the OP: their axons are the first to grow out of the OP at 22-24 hpf, and ablation experiments suggest that they act as a scaffold for the growth of the axons of the later born OSNs, located in the rosette forming in the dorso-lateral region of the OP (Whitlock and Westerfield, 1998). Madelaine et al. (2011) further showed that the first neurons to differentiate in the OP (the early olfactory neurons or EONs) express the *Tg(neurog1:GFP)* transgene (Blader et al., 2003). However, as discussed in Madelaine et al., 2011, *neurog1:GFP*+ neurons appear much more numerous than the previously described pioneer neurons, and may thus include pioneers but also other neuronal subtypes (Whitlock and Westerfield, 1998; Madelaine et al., 2011).

Between 14 and 22 hpf, in a process referred to as OP coalescence, cell movements transform the elongated OP domains into two rounded placodal structures on each side of the brain (Whitlock and Westerfield, 2000). Using the *Tg(neurog1:GFP)* line, it was shown that OP coalescence occurs through two cell movements: first, cell bodies from the anteroposterior extremities of the OP domain converge towards the OP centre. OP cell bodies then move laterally, away from the brain, while their trailing axons remain attached to the brain and grow through retrograde extension (Aguillon et al., 2020; Breau et al., 2017; Monnot et al., 2022). During OP coalescence, *neurog1:GFP*+ cells present in the adjacent forebrain undergo a directional anterior movement (Breau et al., 2017; Monnot et al., 2022).

To analyse Laminin expression at these coalescence stages, we performed immunostainings with a Laminin polyclonal antibody on *Tg(neurog1:GFP)* embryos. Consistent with previous observations (Torres-Paz and Whitlock, 2014; Torres-Paz et al., 2021), we first noticed the appearance of a fairly continuous (with only tiny interruptions) Laminin-rich BM surrounding the brain from 17-18 hpf, while around the OP, only discrete Laminin spots were detected at this stage (**Fig. 1A, A'**). By contrast, at the end of coalescence (22 hpf), two distinct BMs were clearly visible, one around the brain and the other one partially enveloping the OP on its basal side (**Fig. 1B, B'**), suggesting that the Laminin-rich BM of the OP starts to assemble between 18 and 22 hpf, during the late phase of OP coalescence.

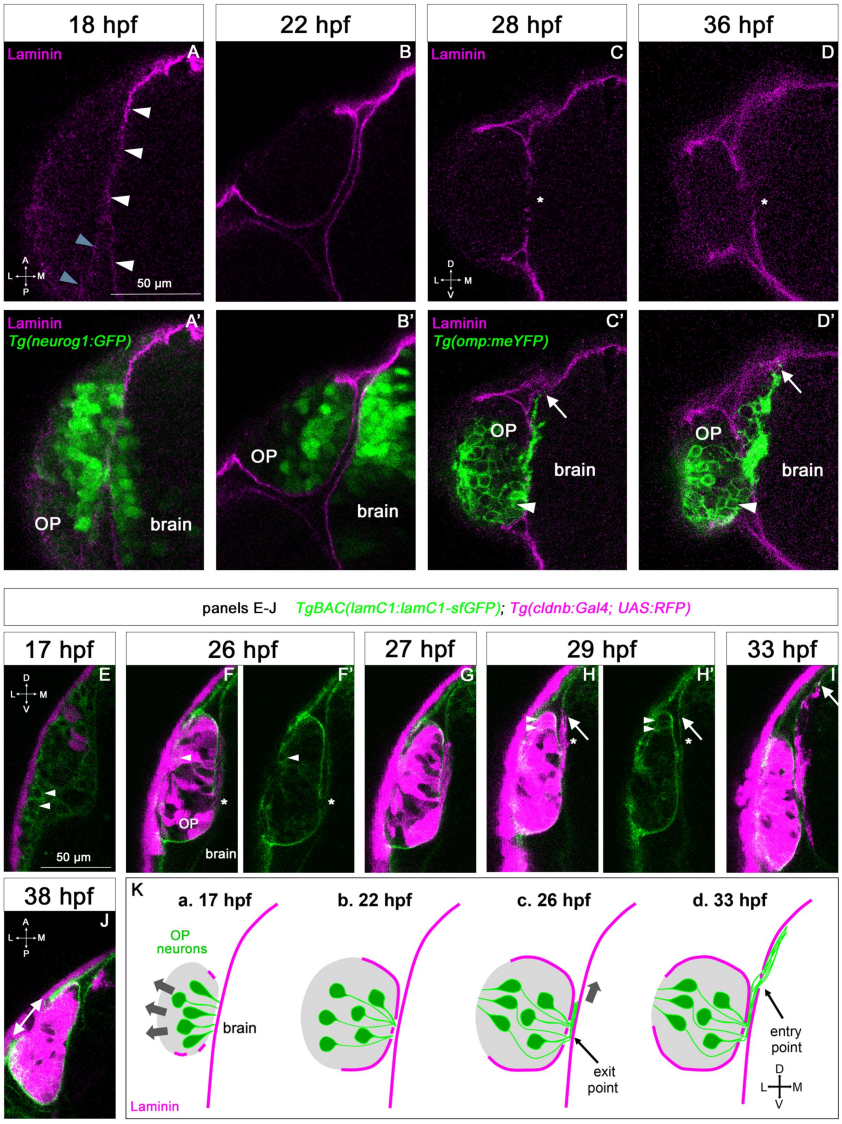

Figure 1.

Expression profile of Laminin in relation with the development of the olfactory system.

A-D. Immunostaining for Laminin (magenta) on *Tg(neurog1:GFP)* embryos (green) at 18 and 22 hpf (A-B', dorsal views), and on *Tg(omp:meYFP)* embryos (green) at 28 and 36 hpf (C-D', frontal views). In A, white arrowheads = BM-like Laminin staining around the brain, grey arrowheads = spotty Laminin accumulation around the OP. In C, D, asterisks = interruptions in the OP's and brain's BM where the YFP+ axons exit the OP and enter the brain. arrows = distalmost extremity of the YFP+ axon bundle, which is in close contact with the internal side of the brain's BM. In C', D', white arrowheads = ventro-medial unipolar neurons labelled by the *Tg(omp:meYFP)* line (see Miyasaka et al., 2005). All the images are single z-sections. **E-J.** Images extracted from confocal live imaging on *TgBAC(lamC1:lamC1-sfGFP); Tg(cldnb:Gal4; UAS:RFP)* embryos (frontal view, except for **Fig. 1J** , dorsal view). LamC1-sfGFP expression in green, and RFP expression (OP cells and peridermal skin cells) in magenta. Arrowheads = OP cells with cytoplasmic LamC1-sfGFP accumulation. Asterisks in F and H = axon exit point and entry point, respectively. Arrows in H and I = distalmost extremity of the RFP+ axon bundle, located close to the brain's BM. In J, double headed arrow = gap in the LamC1-sfGFP observed at the interface with the periderm, where the nostril orifice opens in the skin, as previously reported (Baraban et al., 2023). All the images are single z-sections. **K.** Schematic representation of Laminin-containing BM (magenta) assembly during OP coalescence (a, b), of the formation of the exit/entry points, which often appear as zones with several, small BM interruptions (b, d) and the associated axonal behaviours: retrograde axon extension and lateral movement in the OP (a, b, grey arrows), growth as a fasciculated bundle, initially between the BMs of the OP and the brain (c), and then migration of the axonal tips along the internal side of the brain's BM (d). Scale bar: 50 µm.

To further analyse the dynamics of Laminin γ1 expression and BM assembly during OP coalescence, we took advantage of the *TgBAC(lamC1:lamC1-sfGFP)* line, in which Laminin γ1 is tagged with superfolder GFP and expressed under the control of its own promoter (Yamaguchi et al., 2022). To co-label OP cells, we used the *Tg(cldnb:Gal4; UAS:RFP)* line (Breau et al., 2013), which expresses RFP in all OP cells and in the periderm from around 16 hpf. RFP expression is initially weak and mosaic (**Fig. 1E**) and becomes progressively stronger and more widespread in the OP (**Fig. 1F**). Using confocal live imaging (n = 4 imaged embryos, 2 independent experiments), we confirmed the progressive BM-like accumulation of LamC1-sfGFP around the OP, with a gradual increase of the BM fluorescence during OP coalescence (**Fig. 1E-F'** and Movie 1). From 17 hpf, mesenchymal cells exhibiting cytoplasmic Laminin-sfGFP were seen to migrate anteriorly around the OP (Movie 1). According to the literature, these cells could represent neural crest cells (NCC) (Bryan et al., 2020; Harden et al., 2012; Torres-Paz and Whitlock, 2014) and/or mesodermally-derived cells of the periocular mesenchyme (Vöcking et al., 2023). A subset of RFP+ OP cells also displayed cytoplasmic Laminin-sfGFP (**Fig. 1E-H**' and Movie 1). Altogether, these live imaging experiments suggest that Laminin γ1 around the OP starts to be deposited mostly during late coalescence stages, from at least a subset of OP cells and surrounding mesenchymal cells. Telencephalic cells also exhibited cytoplasmic Laminin-sfGFP expression throughout OP coalescence (Movie 2), suggesting that the forebrain contributes to the deposition of its own Laminin γ1-containing BM at these stages.

To analyse whether the BMs of the brain and OP tissues are maintained at later stages, we used Laminin immunostaining on *Tg(omp:meYFP)* embryos. The *Tg(omp:meYFP)* line labels ciliated OSNs in the dorso-lateral rosette, but also a subset of ventral, unipolar neurons (Miyasaka et al. 2005, see **Figure 1C**', D'). We also used confocal live imaging with the LamC1-sfGFP reporter in the *Tg(cldnb:Gal4; UAS:RFP)* background. Using both approaches we observed a strong, continuous BM-like signal enveloping the brain and the OP at these stages, except (i) where the olfactory axons leave the OP and enter the brain (defined respectively as the exit and entry points, see below) and, as we previously reported (Baraban et al., 2023), (ii) above the neuronal rosette assembling in the dorso-lateral OP, where the nostril orifice opens in the skin (**Fig. 1C-D**', 1F-J). Thus, the OP and adjacent brain tissues are ensheathed by BMs from early stages of olfactory system assembly (as depicted in **Fig. 1K**), suggesting these BMs could play a role in their morphogenesis or the maintenance of their shape during development.

Laminin distribution suggests a role in olfactory axon development

To investigate the distribution of Laminin in relation with axonal development, we used the *Tg(omp:meYFP)* line to visualise olfactory axons including, as described above, the axons of the ciliated OSNs and of a subset of unipolar, ventral neurons (Sato et al. 2005; Miyasaka et al., 2005; Miyasaka et al., 2007). Previous time-course studies using this line showed that following OP coalescence, the YFP+ axons leave the OP from 22-24 hpf through a restricted region in the ventro-medial OP (the exit point), grow dorsally as a fasciculated bundle until around 32 hpf, then start defasciculating in the presumptive olfactory bulb region in the brain (reviewed in Breau and Trembleau, 2023; Miyasaka et al., 2005; Miyasaka et al., 2007; Sato et al., 2007). Immunostaining for Laminin revealed local disruptions in the BMs ensheathing the OP and the brain, precisely where the YFP+ axons exit the OP (exit point) and enter the brain (entry point) (**Fig. 1C-D**'). Once into the brain, from around 28 hpf, the most distal extremity of the YFP+ axon bundle (but not the axon shafts) was systematically in close contact with the Laminin-labelled BM of the brain (**Fig. 1C-D**'), suggesting that the growth cones use it as a substrate to migrate towards the olfactory bulb.

To better understand when and how the gaps of the exit and entry points form in the BMs, we took advantage of our live imaging experiments performed on *TgBAC(lamC1:lamC1-sfGFP); Tg(cldnb:Gal4; UAS:RFP)* embryos (n = 4 embryos, 2 independent experiments). By the end of the

coalescence, when the BM starts to assemble around the OP, we noticed that small interruptions of the BM were already present near the RFP+ axon tips, along the ventro-medial wall of the OP (Movie 2). This was confirmed by live imaging on *TgBAC(lamC1:lamC1-sfGFP); Tg(cldnb:Gal4; UAS:lyn-TagRFP)* embryos (n = 2 embryos), in which OP neurons/axons are mosaically labelled with membrane TagRFP, allowing the visualisation of individual axons (Movie 3). This suggests that the exit point does not open through local perforation of a pre-existing BM around the OP but through incomplete BM synthesis/assembly in this area. The entry point was slightly more dorsal than the exit point (of about 10-20 µm), and the initial dorsal growth of the RFP+ axons thus occurred between the two BMs (**Fig. 1F-H**'). This difference in the z position of the exit and entry points was not clearly seen on fixed embryos (**Fig. 1C-D**'), which we interprete as being a consequence of cell/tissue shape changes due to the fixation process. The opening of the entry point through the brain BM was concomitant with the arrival of the RFP+ axons, suggesting that the axons degrade or displace BM components to enter the brain (**Fig. 1G-H**' and Movie 2). This was also observed by live imaging on *TgBAC(lamC1:lamC1-sfGFP); Tg(cldnb:Gal4; UAS:lyn-TagRFP)* embryos (n = 2 embryos) showing a sparse labelling of OP neurons/axons (Movie 3). Note that, as for the exit points, the entry points often appeared as regions with several, small BM interruptions, rather than as a unique hole in the BM (Movie 4). Once in the brain, as observed in fixed embryos, the distal tip of the RFP+ axons (but not the axon shaft) migrated in close proximity with the brain's BM (**Fig. 1H, I**, Movies 2 and 4). Overall our observations indicate that the axons first grow dorsally for a short distance between the BMs of the OP and the brain, then their distal tips migrate along the internal side of the brain's BM (**Fig. 1K**). We thus hypothesise that the Laminin-rich BMs serve as a migratory path for the axons during their journey from the OP to the olfactory bulb.

The integrity of BMs around the brain and the OP is affected in the *sly* mutant

We used the *sly* mutant to analyse the function of Laminin γ1 in the development of the zebrafish olfactory system. As previously observed (Dolez et al., 2011; Parsons et al., 2002; Stemple et al., 1996; Wiellette et al., 2004), Laminin BM-like accumulation could not be detected in *sly* $^{-/-}$ mutants (referred to as *sly* mutants) at all the analysed stages, from 16 to 36 hpf, while heterozygous *sly* $^{+/-}$ embryos displayed an expression pattern that was similar to *sly* $^{+/+}$ embryos (**Fig. 2A-C**'). This indicates that that there is likely no residual/maternal Laminin at the onset of OP coalescence. Since Laminins are essential for BM assembly in other contexts (Lee and Gross, 2007; Li et al., 2005; Miner and Yurchenco, 2004; Smyth et al., 1999; Urbano et al., 2009), we further checked the presence and structure of the BMs in *sly* mutants. We carried out immunostaining for two other BM components, Collagen IV and Nidogen, at 22, 28 and 36 hpf. Nidogen was present in BM-like structures around the OP and the brain in control siblings, with a pattern resembling that of Laminin, while in *sly* mutants no BM staining could be detected around the two tissues (**Fig. 2D-F**'). In controls, Collagen IV was present in the linear BMs around the OP and the brain, and, with a more fibrous distribution, in the mesenchymal tissues surrounding the OP. In *sly* mutants, Collagen IV immunoreactive pattern was dramatically disrupted, but not totally abolished: the BM-like linear staining was absent, but discrete patches of fibrous expression remained around the OP, at various locations (**Fig. 2G-I**').

We next used electron microscopy (EM) to analyse the ultrastructure of BMs in *sly* mutants and control siblings. We focused on the interface between the forebrain and the OP, where NCC are known to migrate during OP coalescence (Bryan et al., 2020; Harden et al., 2012; Torres-Paz and Whitlock, 2014). NCC, OP and brain cells could be identified on the large field EM images by their position and morphology (**Fig. 2L, L'**). At 24 hpf in controls, the plasma membranes of NCC were separated from those of adjacent OP and brain cells by a 120 nm-wide gap containing electron dense ECM material (**Fig. 2J, M**). This material likely represents the BMs of the two tissues, with morphological features resembling those of BMs found in other tissues of zebrafish embryos at similar stages (Bryan et al., 2020; Yamaguchi et al., 2022). In *sly* mutants, almost

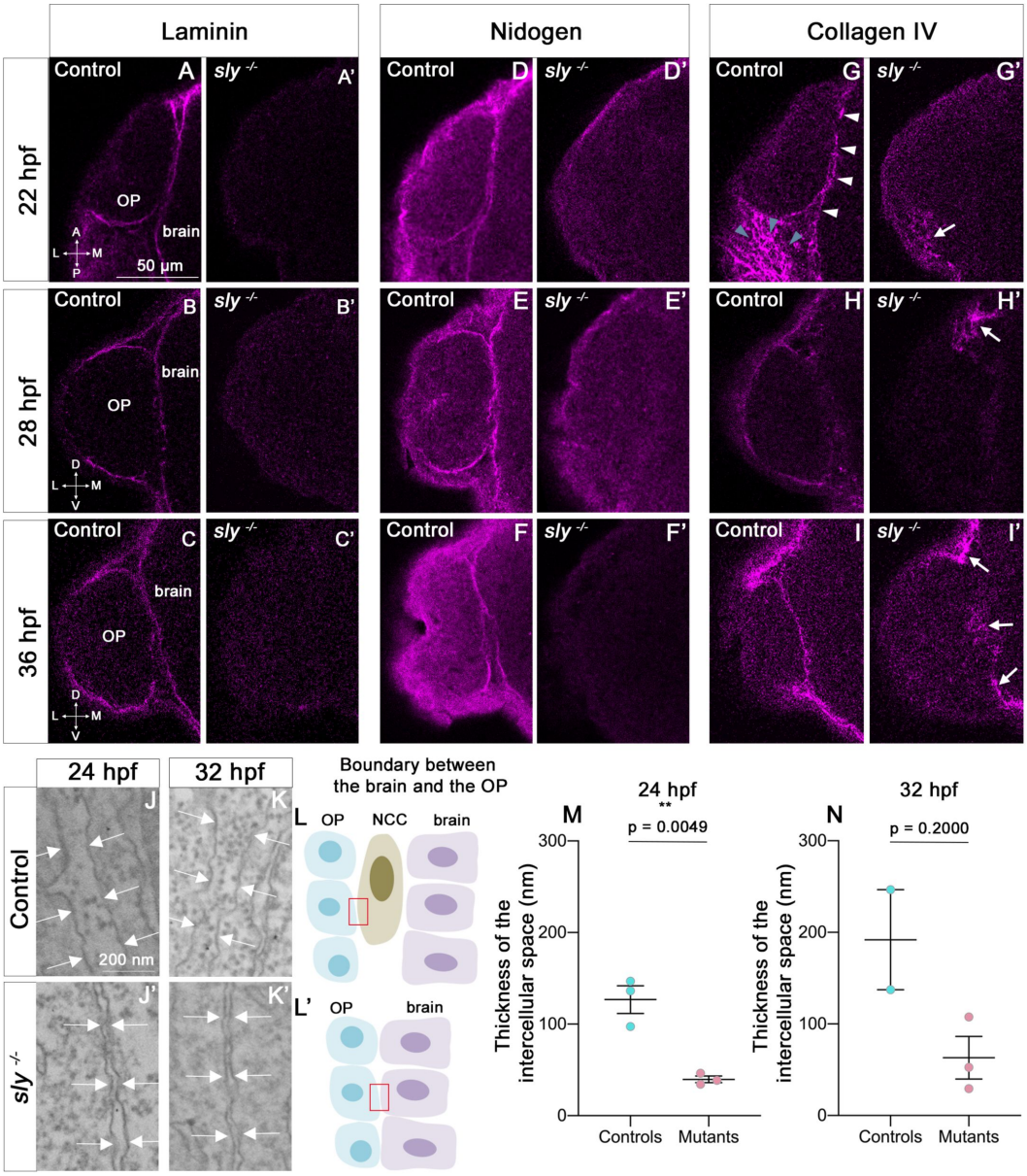

Figure 2.

The integrity of the BMs of OP and brain tissues is strongly affected in *sly* mutants.

A-I. Immunostaining for Laminin (A-C), Nidogen (D-F) and Collagen IV (G-I) (magenta) on *sly* mutants and control siblings at 22 (dorsal view), 28, and 36 hpf (frontal view). For Laminin and Nidogen, the linear, BM-like staining seen in controls around the OP and brain tissues is not detected in *sly* mutants. In G, white arrowheads = BM-like linear Collagen IV staining, grey arrowheads = fibrous staining around the OP. In *sly* mutants, the linear Collagen IV pattern is dramatically disrupted, with, however, remaining fibrous patches of Collagen IV in some discrete areas located at the margin of the OP and/or between the OP and brain (arrows in G', H', I'). Scale bar: 50 µm. **J, K**. Examples of EM images of the intercellular space between NCC and the OP in control siblings (J, K) and the OP and the brain in *sly* mutants (J', K'), at 24 (J, J') and 32 hpf (K, K'). Arrows = plasma membranes. The pictures were taken in the areas depicted with red boxes in L, L'. **L.** Schematic view of the brain/OP boundary and of the areas (red boxes) where the pictures were taken in controls (L) and *sly* mutants (L'). OP, brain and NCC were identified by their position and shape: migrating NCC showed an elongated morphology along the AP axis, which differed from the round OP cell bodies and from brain neuroepithelial cells elongated along the ML axis. **M, N.** Thickness of the intercellular space in *sly* mutants (between OP and brain cells) and control siblings (between NCC and brain or OP cells) at 24 hpf (n = 3 controls; n = 3 mutants) and 32 hpf (n = 2 controls; n = 3 mutants). For 24 hpf, unpaired, two-tailed t test. For 32 hpf, Mann-Whitney test.

no NCC could be detected, suggesting that NCC development is affected. In this mutant context, the plasma membranes of OP and brain cells were separated by a 40 nm-wide gap, which was significantly smaller than in controls. This gap was most often devoid of electron dense material (only rare spots could be detected, **Fig. 2J, J', M**). A similar trend was detected at 32 hpf (**Fig 2K, K', N**). By contrast, the thickness of the intercellular gaps within the OP or the brain was not affected in mutants (Fig. S1). The integrity of the OP and brain BMs is thus strongly affected in *sly* mutants, as previously reported in other tissues of Laminin γ1 mutants (Urbano et al., 2009; Yamagushi et al., 2022). We next analysed the consequences on the development of the olfactory system components (placode, brain, olfactory axons).

OP coalescence still occurs in the *sly* mutant

To study the role of Laminin γ1-dependent BMs in OP coalescence, we first measured the dimensions of the *Tg(neurog1:GFP)*+ OP cell clusters at 22 hpf (end of coalescence) on fixed *sly* mutants and control siblings. While no difference was found for anteroposterior (AP) and dorsoventral (DV) dimensions, the mediolateral (ML) dimension was increased in mutants (**Fig. 3A-E**). This could be the consequence of an increased number of GFP+ cells, however no difference was found in the number of mitotic cells in the OPs of *sly* mutants and control siblings at 16 and 21 hpf (Fig. S2A, B, E, F) and, as previously reported in other tissues (Parsons et al., 2002), we observed a tendency for the *sly* mutants to exhibit increased apoptosis (Fig. S2I, J, M, N). The higher ML dimension could also be due to increased lateral movements of OP cell bodies in the absence of the BM surrounding the OP. To test this, we performed live imaging on *sly* mutants and control siblings carrying the *Tg(neurog1:GFP)* transgene, mounted in a dorsal view (n = 5 mutants and n = 5 controls) (**Fig. 3F-I** and Movie 5). Individual nuclei of GFP+ OP and brain cells were tracked using widespread expression of H2B-RFP, obtained through mRNA injection. From the cell trajectories we extracted the 3D Mean Square Displacements (MSD), a measure of the volume explored by a cell in a given period of time. No significant difference was observed for the MSD of OP cells between controls and *sly* mutants, but the MSD was higher for brain cells in the mutants (**Fig. 3J, K**). Direction wise, surprisingly OP cells did not show any change in their total ML displacement (**Fig. 3L**), nor in their DV displacement (**Fig. 3M**). Differences, although not statistically significant, could be detected along the AP axis for anterior, central and posterior OP cells: in the mutants the anterior cohort of cells tended to migrate less posteriorly, while central and posterior cells migrated more anteriorly, as if the final cell positions were all shifted towards more anterior locations (**Fig. 3N-P**). In conclusion, while the movements of brain cells are increased in the absence of BMs at coalescence stages, overall the OP cell movements occur with normal parameters and allow the condensation of OPs into compact neuronal clusters in the *sly* mutants. It is possible however that the position of the OP along the AP axis is shifted anteriorly at the end of OP coalescence.

Role of Laminin γ1-dependent BMs during the forebrain flexure

Following OP coalescence, the forebrain flexure, a major morphogenetic process which is essential for the final folded shape of the vertebrate brain, starts to remodel the head tissues (Chapman et al., 2005; Garcia et al., 2017; Hauptmann and Gerster, 2000; Tropepe and Sive, 2003). In zebrafish the bending of the forebrain has been reported to occur between 24 and 48 hpf through the observation of fixed samples (Ross et al., 1992; Hauptmann and Gerster, 2000). We set out to investigate the role of the brain and OP BMs during the forebrain flexure. The *Tg(omp:meYFP)* transgene expression was used to quantify the dimensions of the YFP+ cluster in the OP at various stages of the flexure (24, 28, 32 and 36 hpf). While no change could be detected in the AP and ML dimensions of the YFP+ cluster (except for the ML dimension at 28 hpf), its DV dimension was significantly increased in *sly* mutants at all the analysed stages (**Fig. 4A-E** and Fig. S3A-L). This higher DV dimension is unlikely to result from an increase in the number of cells, since YFP+ mitotic cells were not more numerous in *sly* mutants (Fig. S2C, D, G, H), and YFP+ OP clusters displayed increased apoptosis, as observed at earlier stages (Fig. S2K, L, O, P). Counting the YFP+

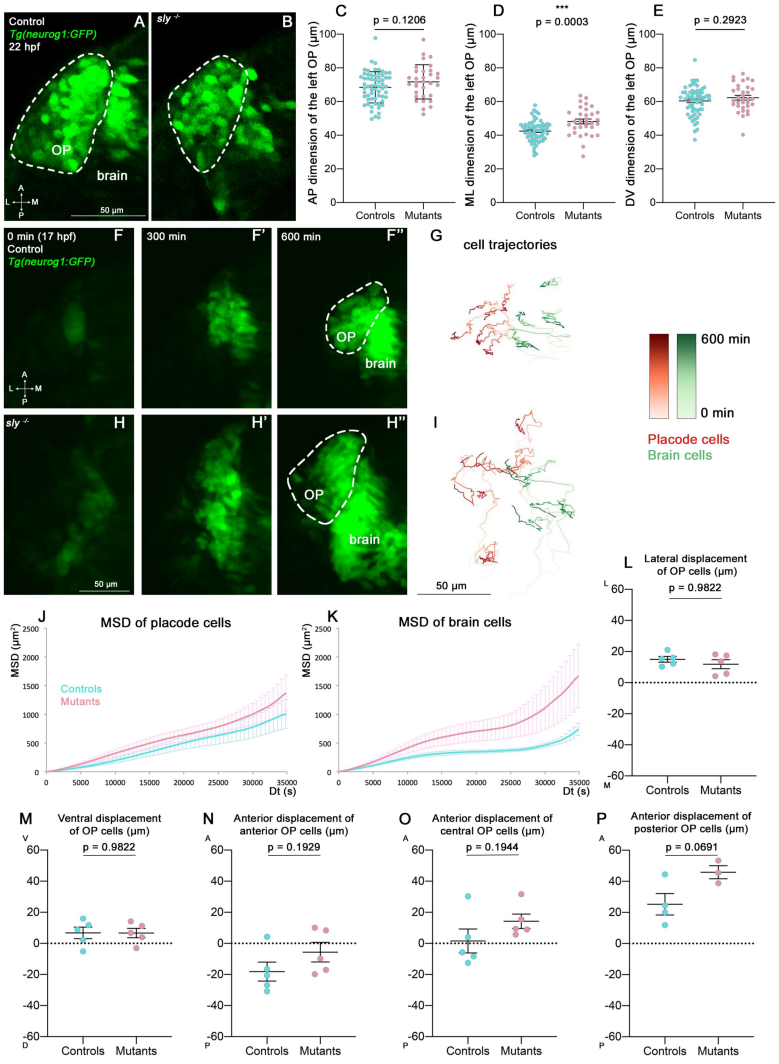

Figure 3.

Analysis of OP coalescence in *sly* mutants and control siblings.

A, B. Images (dorsal views, 1 z-section) of representative OPs from a *Tg(neurog1:GFP); sly* $^{-/-}$mutant (right) and a control *Tg(neurog1:GFP)* sibling (left) at the end of OP coalescence (22 hpf). The *Tg(neurog1:GFP)*$^{+}$ OP clusters are surrounded by dotted lines. **C-E.** Graphs showing the anteroposterior (AP, in C), the mediolateral (ML, in D), and dorsoventral (DV, in E) dimensions of the *Tg(neurog1:GFP)*$^{+}$ OP clusters in *sly* mutants (pink) and control siblings (blue) at 22 hpf (n = 62 controls and n = 32 mutants from 2 independent experiments). Ectopic fluorescent cells (cells that are physically separated from the main cluster) were not taken into account for the measurement of OP dimensions. Unpaired, two-tailed t test. **F-F'' and H-H''.** Images extracted from confocal live imaging on *Tg(neurog1:GFP)* control (F-F'') and *sly* mutant (H-H'') embryos during OP coalescence, dorsal view, average projection. Only the left side of the embryo is shown. **G, I.** Examples of 2D tracks (ML along X and AP along Y) of *Tg(neurog1:GFP)*$^{+}$ OP cells (red) and *Tg(neurog1:GFP)*$^{+}$ brain cells (green) in a control (G) and a *sly* mutant embryo (I). Only the left side of the embryo is shown. The time is color-coded: light colors at the beginning of the trajectory (17 hpf) towards dark colors for the end of the track (600 min later). **J, K.** MSD analysis for OP cells (J) and brain cells (K) in *sly* mutants and control siblings (n = 5 controls and n = 5 mutants from 3 independent experiments, 10 to 14 cells analysed in each tissue). **L, M.** Graphs showing the total lateral (L) and ventral (M) displacement of OP cells, starting at 17 hpf and during 600 min of time lapse (n = 5 control placodes and n = 5 mutant placodes from 3 independent experiments, 10 to 14 cells per placode, unpaired, two-tailed t test). **N-P.** Graphs showing the total anterior displacement of anterior, central and posterior OP cells (as defined in Breau et al., 2017), starting at 17 hpf and during 600 min of time lapse (n = 5 control placodes and n = 5 mutant placodes from 3 independent experiments, mean calculated from 1 to 12 cells per placode, unpaired, two-tailed t test). Note that in some of the OPs we could not find any trackable (i.e. expressing H2B-RFP) posterior OP cell, which explains why there are only 4 control points and 3 mutant points in the graph showing the anterior displacement of posterior cells).

cells on high magnification images of 3 mutant and 3 control OPs at 28 and 36 hpf further confirmed that the YFP+ cell number is unchanged (Fig. S2Q, R). In addition to the DV elongation of the OP tissue, isolated, ectopic (mispositioned) YFP+ cells were observed all around the YFP+ cluster in the *sly* mutants (**Fig. 4F-H** and Movie 8). The rosette structure appeared to form normally on the dorso-lateral region of the OP in *sly* mutants (Movie 8).

To better understand the origin of these phenotypes, we analysed the dynamic behaviours of brain and OP cells occurring during the forebrain flexure, which had not been characterised so far. We carried out live imaging from 22 to 40 hpf on *Tg(omp:meYFP) sly* mutants and control siblings injected with H2B-RFP mRNA to label all nuclei, and tracked YFP+ OP cells and adjacent brain cells (n = 4 mutants and n = 4 controls) (**Fig. 4I-L** and Movie 6). From 24-26 hpf we observed a marked anterior and ventral departure of brain cells in control embryos, representing the onset of the flexure movement. Strikingly, OP cells also moved anteriorly and ventrally from these stages, in coordination with the brain, revealing that the OPs are also subjected to the flexure movement (**Fig. 4J** and Fig. S3M, Movie 6). The flexure movements were also visible in the brain and OPs of *sly* mutants (**Fig. 4L** and Fig. S3N, Movie 6), with OP cells moving with a higher MSD than in controls (**Fig. 4M**). A similar trend was observed for brain cells, but was not statistically significant (**Fig. 4N**). Moreover, upon visualisation of the cell trajectories in a lateral (YZ) view, we noticed that in 4/4 mutant embryos, brain and OP cells exhibited curved trajectories, moving first anteriorly and ventrally, then turning posteriorly, while this phenomenon occurred in only 1/4 control sibling during the duration of our movies (Fig. S3M, N). This reinforces the idea that brain and OP cells are subjected to an accelerated or enhanced forebrain flexure remodelling in the *sly* mutants, and suggests that in the wild type situation the BMs allow the tissues, and in particular the OP, to resist to the morphogenetic movements associated with the flexure. Altogether, our findings show that the Laminin γ1-containing BMs are required to prevent OP cell scattering, maintain OP shape and dampen OP cell movements during the forebrain flexure.

Laminin γ1-dependent BMs are required to define a robust boundary between the OP and the brain

OP cells undergo anterior and ventral movements during the forebrain flexure. We noticed that, while in control siblings OP cells also display a lateral displacement, they rather move in the medial direction in *sly* mutants, towards the brain, as if the two OPs were progressively converging towards each other (**Fig. 4J, L, O**). This prompted us to image OP and brain tissues in 3D to visualise the boundary between the two tissues and analyse the width of the brain. To do so, we first performed immunostainings at 28 and 36 hpf for the pan-neuronal marker HuC to visualise neurons in the OP and brain on *Tg(cldnb:Gal4; UAS:RFP)* embryos, in which RFP is expressed in the OP. Qualitative observations of these z-stacks revealed that OPs in *sly* mutants are partially embedded within the brain tissue and display a curved and irregular boundary with the brain, while the frontier between the two tissues appears as a straight line in control siblings (**Fig. 5A, A'**, Fig. S4A, A' and Movie 7). To quantify the width of the brain, we used the *Tg(eltC:GFP)* line (Stedman et al., 2009), which expresses GFP in forebrain cells, and crossed it with the *Tg(cldnb:Gal4; UAS:RFP)* line to label the OPs (**Fig. 5B, B'** and Fig. S4B, B'). We measured the width of the forebrain in 3 distinct AP levels and 3 distinct DV levels in between the two OPs (as depicted in **Fig. 5B, B'** and Fig. S4B, B' for the DV levels). The width of the forebrain in *sly* mutants was smaller than in controls, in particular in anterior and dorsal areas (**Fig 5B-D** and Fig. S4B-D). Proliferation was unchanged in the brain of *sly* mutants, while apoptosis was only sligtly increased (Fig. S4E-L), suggesting that the smaller brain width is due to a local distortion of the tissue rather than a decreased number of cells. Next, we quantitatively analysed the straightness of the brain/OP boundary. Note that the *Tg(eltC:GFP)* line could not be used for that purpose because a few cells in the OP also express the transgene. In addition, *Tg(cldnb:Gal4; UAS:RFP)* expression is mosaic in the OP, preventing the use of this line to assess the shape of the brain/OP boundary. To perform such a quantification we thus turned to immunostainings for Dlx3b, a transcription factor specifically expressed in OP (and skin) cells (Torres-Paz and Whitlock,

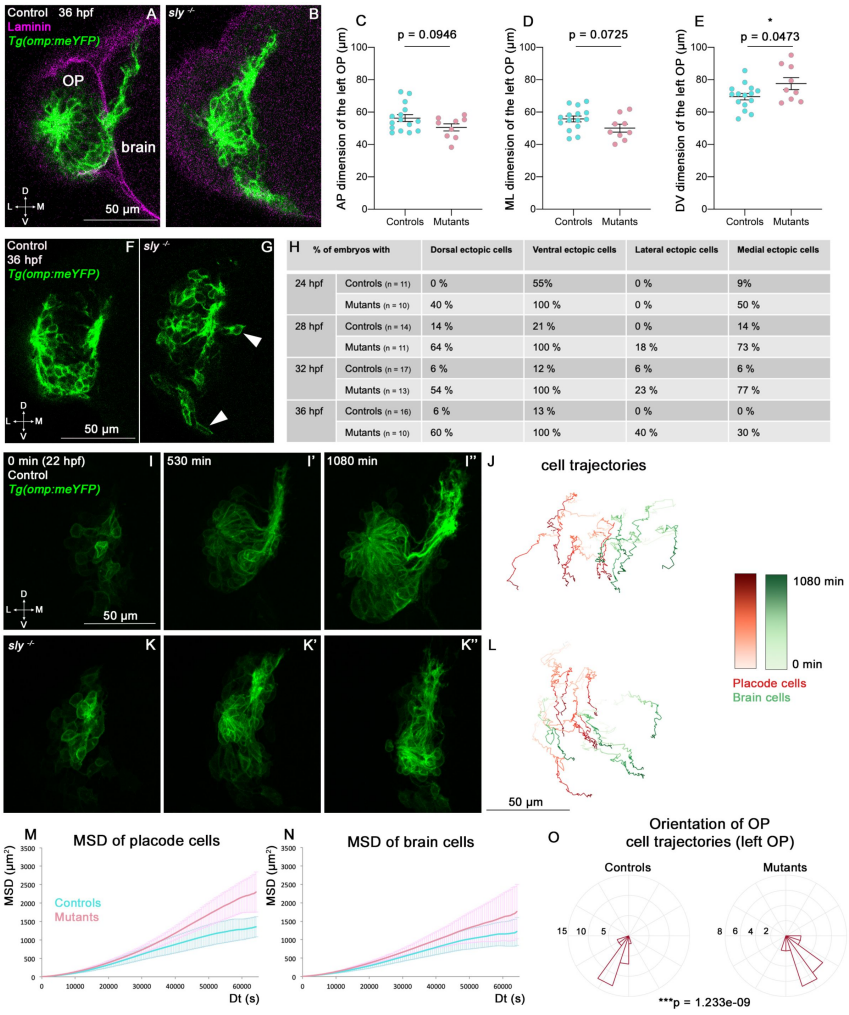

Figure 4.

Analysis of OP and brain morphogenesis in *sly* mutants and control siblings during the forebrain flexure.

A, B. Images (frontal view, 1 z-section) of representative placodes from a *Tg(omp:meYFP); sly* $^{-/-}$ mutant (right) and a control *Tg(omp:meYFP)* sibling (left) at 36 hpf. Laminin immunostaining in magenta. **C-E.** Graphs showing the anteroposterior (AP, in C), the mediolateral (ML, in D), and dorsoventral (DV, in E) dimensions of the *Tg(omp:meYFP)*$^{+}$ OP clusters in *sly* mutants (pink) and control siblings (blue) at 36 hpf (n = 15 controls and n = 9 mutants from 4 independent experiments). Ectopic fluorescent cells (cells that are physically separated from the main cluster) were not taken into account for the measurement of OP dimensions. Unpaired, two-tailed t test. Similar measurements performed at younger stages are shown in Fig. S3A-L. **F, G.** Examples of images used for the analysis of ectopic cells, defined as *Tg(omp:meYFP)*+ cells being physically separated from the main YFP+ cluster. Arrowheads show instances of ectopic cells in a *sly* mutant. **H.** Table showing the % of control and mutant embryos with at least one ectopic cell located dorsally, ventrally, laterally, and medially to the main YFP+ cluster. The numbers of analysed embryos are indicated in the table. **I-I'' and K-K''.** Images extracted from confocal live imaging on *Tg(omp:meYFP)* control (I-I'') and *sly* mutant (K-K'') embryos during the forebrain flexure, from 22 hpf and over 1080 min, frontal view, maximum projection. Only the left side of the embryo is shown. **J, L.** Examples of 2D tracks (ML along X and DV along Y) of *Tg(omp:meYFP)*$^{+}$ OP cells (red) and adjacent brain cells (green) in a control (J) and a *sly* mutant (L). The time is color-coded: light colors at the beginning of the trajectory (22 hpf) towards dark colors for the end of the track (1080 min later). Only the left side of the embryo is shown. **M, N.** 3D MSD analysis of OP (M) and brain cells (N) in *sly* mutants and control siblings (n = 4 controls and n = 3 mutants from 5 independent experiments, 10 to 14 cells analysed in each tissue). **O.** Rose plots indicating the orientation of the movement for control and mutant left OP cells (data pooled from n = 4 controls and n = 3 mutants from 5 independent experiments). Numbers = number of cells. Dorsal to the top, lateral to the left. There is a statistical difference in cell track orientations between controls and mutants (circular analysis of variance based on the likelihood ratio test: p = 1.233e-09 for the left OPs, and p = 3.439e-08 for the right OPs, the graphs for the rigth OPs are not shown).

2014). We used deep learning to segment the 3D z-stacks of Dlx3b-immunostaining in control and *sly* mutant embryos at 36 hpf (**Fig. 5E-F'**), and quantified the distortion of the OP/brain frontier at various z levels. This analysis demonstrated that the OP/brain boundary is less straight in *sly* mutants as compared with controls (**Fig. 5G, H**). Thus, our analyses of cell tracks, brain size and proliferation/apoptosis, and of the shape of the brain/OP boundary suggest that the forebrain is smaller and distorted in *sly* mutants, possibly due to the inward convergence of the two OPs. An non-mutually alternative hypothesis is that the brain fails to form in the normal size and shape in *sly* mutants. These findings suggest that the Laminin γ1-dependent BMs serve to establish a straight brain/OP boundary preventing local intermixing and the late convergence of the two OPs towards each other during the flexure movement.

Role of Laminin γ1-dependent BMs in olfactory axon development

The growth of the olfactory axons starts with the retrograde axon extension of their proximal portions during OP coalescence, from 14 to 22 hpf (Breau et al., 2017), followed by the dorsal growth from the brain/OP boundary to the olfactory bulb from 22 to 32 hpf (**Fig. 1K**). Laminin has been reported to orient the emergence of axons (Randlett et al., 2011; Moore et al., 2022). Do the Laminin γ1-dependent BMs play any role in axon emergence or anchoring during retrograde axon extension? To test this, we performed live imaging experiments during OP coalescence on *Tg(cldnb:Gal4; UAS:RFP)* embryos injected with the *neurog1:GFP* plasmid (Blader et al., 2003), allowing a sparse labelling of *neurog1:GFP*+ axons (n = 4 mutants and n = 4 controls, 2 independent experiments). Several instances of retrograde extension were seen both in controls and mutants (Fig. S5A, B), indicating that retrograde axon extension occurs normally for at least some of the *neurog1:GFP*+ neurons/axons in *sly* mutants. In addition, on fixed *Tg(omp:meYFP)* *sly* mutants at 24 hpf, numerous YFP+ neurons had their proximal axonal portion formed and attached to the brain surface (Fig. S5C-F), suggesting that retrograde axon extension also occurs normally for at least some of the YFP+ OP neurons. Although we can not rule out that retrograde axon extension is affected in a subset of OP neurons, for instance in ectopic cells, the presence of a BM around the OP and/or the brain appears not to be an absolute requirement for the attachment of axon tips to the ventro-medial wall of the OP during retrograde extension.

Are Laminin γ1-dependent BMs important for the growth or navigation of the axons from the brain/OP boundary to the olfactory bulb, as suggested by Laminin expression? We first examined the axons in *Tg(omp:meYFP)* embryos at 24, 28, 32 and 36 hpf. In mutant embryos, severe axonal defects were observed. Most YFP+ axonal protrusions were unable to leave the OP and appeared to stall at the OP/brain boundary, leading in some embryos to an apparent absence of axon bundle (Fig. S5G, left column and Movie 8). In some embryos (8-10%), a small proportion of axons managed form a bundle reaching the presumptive OB region by ectopically exiting the OP dorsally (an exit point location never observed in the control fish), while the axons would normally exit the OP at a more ventro-medial position in the controls (Fig. S5G, left column and Movie 8). In addition, an increased proportion of embryos with ectopic medial projections was observed in mutants (18 to 30% of the embryos depending on the stage, as compared to 0 to 9% in controls, Fig. S5G, right column). Finally, there is a tendency for a higher percentage of embryos displaying ventral projections in the *sly* mutant, particularly visible at 24 hpf (Fig. S5G, middle column). Altogether, these results suggest navigation issues.

So far the growth of the zebrafish olfactory axons from the OP to the bulb has been mostly characterised using fixed samples or live imaging with long time intervals (Dynes and Ngai, 1998; Miyasaka et al., 2007). To analyse the dynamic behaviour of the axons, we performed live imaging from 22 hpf on *sly* mutant and control embryos injected with the *omp:meYFP* plasmid, in order to obtain a mosaic labelling of the YFP+ neurons and their axons (n = 5 mutants and n = 5 controls, **Fig. 6A, B**). We tracked individual YFP+ growth cones, as well as the YFP+ cell bodies in the OP, during consecutive periods of 200 min each, with a time interval of 10 min. We substracted the average movement of OP cell bodies from the growth cone tracks, in order to

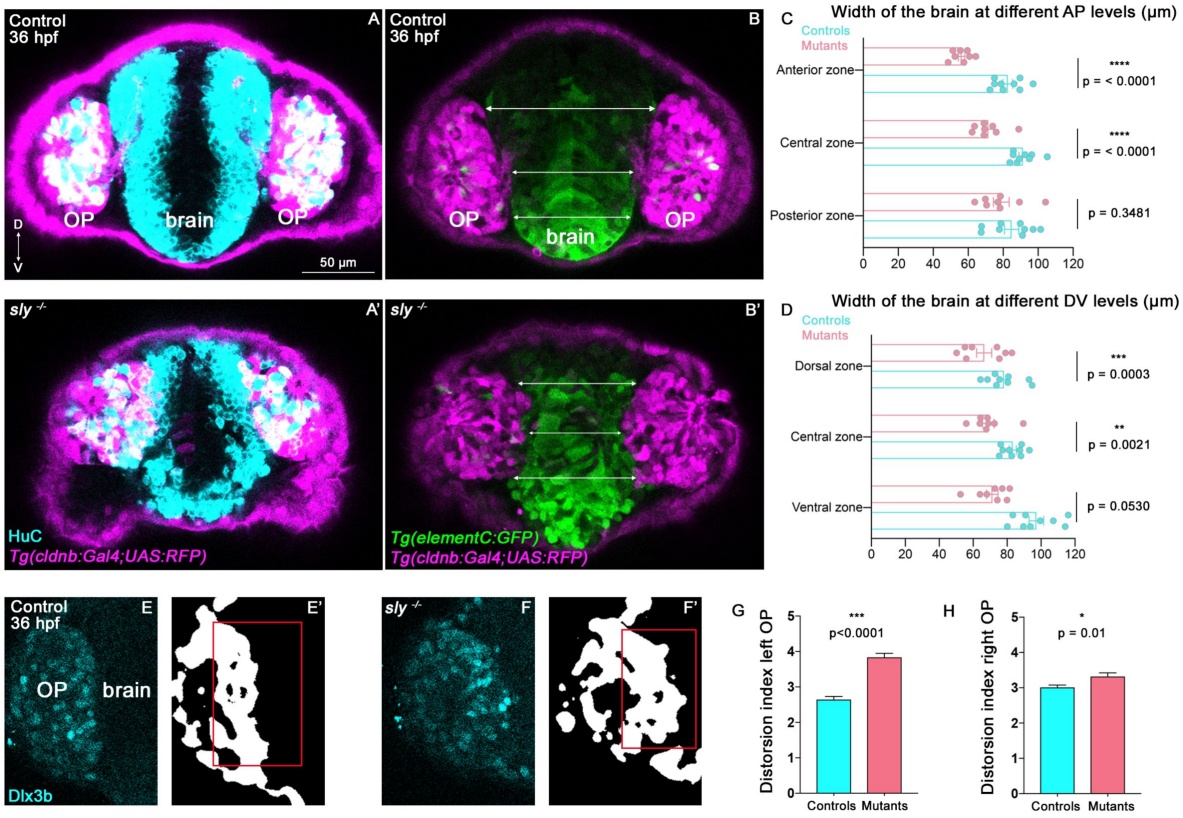

Figure 5.

Analysis of brain width and brain/placode boundary in *sly* mutants and control siblings.

A, A'. Immunostaining for HuC (cyan) at 36 hpf on *Tg(cldnb:Gal4; UAS:RFP)* (magenta) control and *sly* mutant embryos (frontal view). Similar immunostainings performed at 28 hpf are shown in Fig. S4A, A'. **B, B'**. Images of *Tg(elementC:gfp); Tg(cldnb:Gal4; UAS:RFP)* control and mutant embryos at 36 hpf (frontal view), similar images acquired at 28 hpf are shown in Fig. S4B, B'. GFP (green) is expressed by the forebrain and a few OP cells. Arrows indicate where the brain width was measured (in 3 distinct positions along the DV axis). Measurements were also carried out at 3 distinct AP levels (through the z-stack). **C, D.** Width of the forebrain in 36 hpf controls and *sly* mutants, at 3 different DV and 3 different AP levels (n = 9 controls and n = 8 mutants from 4 independent experiments, unpaired, two-tailed t test). Quantifications for the 28 hpf stage are shown in Fig. S4C, D. **E-F'.** Immunostaining for the OP marker Dlx3b (cyan) was performed on 36 hpf *sly* mutants and control siblings (frontal view). The signal was segmented using deep learning approaches (white signal), and the distortion index (see Material and Methods) of the OP/brain boundary was calculated in the regions outlined with red boxes. **G, H.** Graphs showing the distortion indexes in controls and mutants at 36 hpf, for the left and right OPs (n = 3 controls and n = 3 mutants). ANOVA test (mixed models, with animals as random effect and genotype and side as fixed effects).

remove the contribution of the global flexure remodelling and analyse specifically the behaviours of the axons with respect to the surrounding cells/tissue. In controls, as expected, growth cones overall showed a dorsal and medial migration, except at the end of the movie, which likely corresponds to their arrival and stalling in the presumptive olfactory bulb. By contrast, growth cones in the *sly* mutants did not display a directional migration towards the bulb, during the whole movie duration (**Fig. 6C, F, I, L**). They were motile and explored the environment, as shown by speed and persistence measurements, but moved on short distances and/or without preferential direction, resulting in a perturbed axon growth (**Fig. 6C-N**). These live imaging analyses confirm that the migration of the olfactory axons is impaired in *sly* mutants. Altogether, our results show that Laminin γ1-dependent BMs are essential for the growth and navigation of the axons from the OP to the olfactory bulb.

Sly mutants display cranial NCC defects but this does not contribute to the late olfactory system phenotypes

Cranial NCC migration is concomitant with OP coalescence. From 14 hpf, NCC progressively populate the gaps between the OP and the eye and brain tissues (Harden et al., 2012; Torres-Paz and Whitlock, 2014; Bryan et al., 2020). Our electron microscopy observations suggested that NCC are absent at the brain/OP interface of *sly* mutants. *In situ* hybridisation for the NCC marker *crestin* (Luo et al., 2001) revealed that, while a clear NCC cluster can be seen at the brain/OP interface in controls at 32 hpf, *crestin*-labelled NCC are absent from this area in *sly* mutants (Fig. S6A, A'). This suggests that Laminin γ1-dependent BMs are important for NCC migration or survival in this region of the embryo.

To analyse the dynamics of NCC migration in *sly* mutants and control siblings, we performed live imaging from 16 to 32 hpf on embryos carrying the *Tg(neurog1:GFP)* and *Tg(UAS:RFP)* transgenes and injected with a *sox10(7.2):KalTA4* plasmid (Almeida et al., 2015), which allows the mosaic labelling of NCC (n = 10 control placodes and n = 8 mutant placodes, 3 independent experiments) (Movie 9). As expected from previous studies (Harden et al., 2012; Torres-Paz and Whitlock, 2014, Bryan et al., 2020), in 10/10 control placodes many labelled NCC had already reached the vicinity of the OP at 16 hpf, and further invaded the interface between the eye and the OP during the movies (Fig. S6B). Surprisingly, in *sly* mutants, numerous motile NCC were also observed close to the OP at 16 hpf in all the analysed placodes (8/8), and populated the eye/OP interface in 7/8 placodes (10/10 in controls) (Fig. S6B). In a subset of control placodes we could detect a few NCC populating the forebrain/OP interface, either ventrally (4/10 placodes) or dorsally (8/10 placodes). By contrast, in *sly* mutants, NCC were observed in the dorsal region of the brain/OP boundary in only 2/8 placodes, and in the ventral brain/OP frontier in only 2/8 placodes as well. Interestingly, in these two samples, NCC that had initially populated the ventral brain/OP interface were then expelled from the boundary at later stages (Movie 9 and Fig. S6B). Altogether, these live imaging data suggest that the migration of cranial NCC towards the OP and between the eye and OP is only partially impaired in *sly* mutants. The subset of NCC that populate the OP/forebrain appears to be more specifically affected, with defects in their migration to the interface and/or the maintenance of their position at the interface. Note that since the *crestin* marker labels mostly NCC at the OP/forebrain interface at 32 hpf (Fig. S6A), this could explain why *crestin* expression is almost lost in *sly* mutants at this stage.

To test whether the phenotypes observed in *sly* mutants are linked to NCC defects, we took advantage of the *foxd3* mutant, in which cranial NCC migration is delayed (Bryan et al., 2020; Monnot et al. 2022), leading to a loss of *crestin*-labelled NCC at 32 hpf which resembles that of the *sly* mutants (Fig. S7A, B). Importantly, Laminin expression appeared to be unchanged in *foxd3* mutants (Fig. S7C', D' and Monnot et al., 2022). We previously showed that this mutant displays a slightly higher (of about 8-10 µm) ML dimension of the OP at the end of coalescence (Monnot et al., 2022) which is similar to what we observed in *sly* mutants (**Fig. 3D**). This suggests that

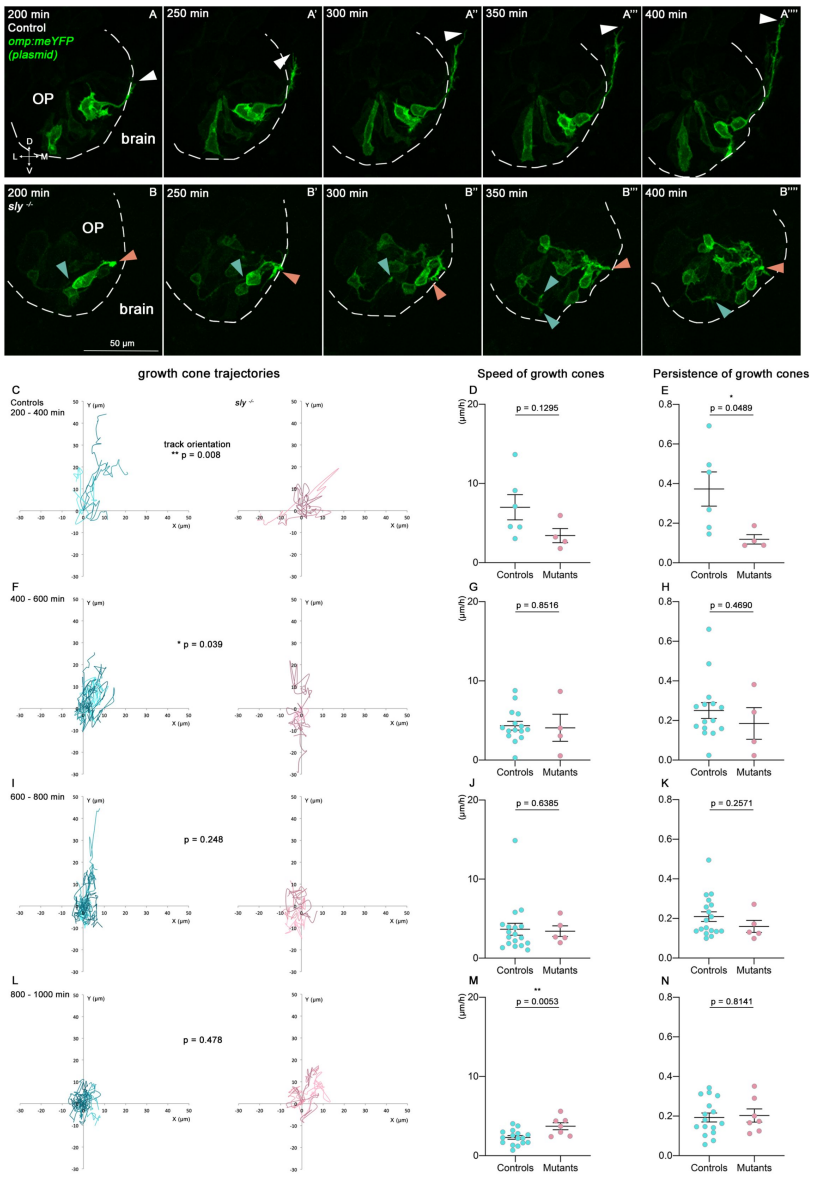

Figure 6.

Quantitative live imaging of axonal behaviours in *sly* mutants and control siblings.

A, B. Images extracted from confocal live imaging on control (A-A'''') and *sly* mutant (B-B'''') embryos injected with the *omp:meYFP* plasmid to obtain a mosaic labelling of OP neurons and their axons (frontal view, maximum projections). The OP neurons and their axons were imaged every 10 min over 1000 min from 22 hpf. Here, only the 200-400 min time window is shown as an example. Arrowheads = positions of individual growth cones over time. **C-N**. Individual YFP+ growth cones, as well as YFP+ cell bodies in the OP, were tracked during 4 consecutive periods of 200 min each (from 200 min of imaging, since before no growth cone could be detected, n = 5 mutants and n = 5 controls from 6 independent experiments). The mean movement of OP cell bodies was substracted from the growth cone tracks to get rid of the global flexure movement. 200-400 min: 6 growth cones in controls, 4 in mutants; 400-600 min: 15 growth cones in controls, 4 in mutants; 600-800 min: 18 growth cones in controls, 4 in mutants; 800-1000 min: 16 growth cones in controls, 7 in mutants. **C, F, I, L**. Tracks of the growth cones merged at their origin for the 4 consecutive periods of 200 min. For each time window, the difference in the orientation of the tracks was analysed using the circular analysis of variance based on the likelihood ratio test. **D, G, J, M.** Mean speed of the growth cones. Unpaired, two-tailed t tests. **E, H, K, N.** Persistence of the growth cones, defined as the distance between the initial and final positions of the growth cones divided by the total length of their trajectory. Unpaired, two-tailed t tests, except for the analysis of the persistence at 400-600 min, and for the speed and persistence at 600-800 min, where Mann Whitney tests were performed.

NCC defects could be the cause of the increased ML dimension in *sly* mutants. We hypothesize that with less NCC around the OP at this stage, the OP tissue is less constrained and thus slightly spread along the ML axis. To further investigate the influence of NCC on the development of the olfactory system at later stages, we analysed OP dimensions and the length of the olfactory axon bundle at 28 and 36 hpf, in *foxd3*$^{-/-}$ mutants and *foxd3* $^{+/-}$ or $^{+/+}$control siblings expressing the *Tg(omp:meYFP)* transgene. No significant difference was observed between controls and *foxd3*$^{-/-}$ mutants for these parameters (Fig. S7C-L), suggesting that the late OP morphogenesis and axonal phenotypes of the *sly* mutants are not a consequence of the impairment of NCC development.

Discussion

Our study highlights key roles of Laminin γ1-dependent BMs in critical aspects of the development of the zebrafish olfactory system, revealed here through the detailed analysis of the Laminin γ1 loss-of-function mutant *sly*. During the late development of the OP, Laminin γ1-dependent BMs turned out to be essential to maintain its shape and proper position, and to establish a robust brain/placode boundary. In addition, Laminin-dependent BMs also appeared to be instrumental to ensure a proper growth and pathfinding of the olfactory axons towards the developing olfactory bulb. In the following paragraphs, we will discuss these new roles assigned to BMs in the context of the development of the zebrafish olfactory system, in light of the literature.

The BM of the OP acts as a "shell" maintaining its shape and proper position in the face of forebrain flexure movements

Our data document a mild perturbation of cell movements during OP coalescence, which suggests that Laminin γ1-dependent BMs are overall dispensable for the OP to acquire its initial shape. However, our observation that the OP of the *sly* mutant becomes significantly elongated in the DV dimension and is surrounded by ectopic cells during the forebrain flexure provides strong evidence for a role of the BMs in preventing OP deformation and scattering during this major remodelling of the head tissues. We discovered, along our live imaging observations, a joint anterior and ventral movement of the OPs and forebrain during the flexure time period in the control animals, as if the OPs were dragged along in the same antero-ventral movement as the forebrain. We thus propose that the BM of the OP prevents its deformation in response to the mechanical forces generated by the morphogenetic movement of the neighboring brain.

The ability of the placode's BM to limit the deformation of the OP during this developmental step most probably relies on its stiffness. In the *Drosophila* egg chamber, while Laminin itself has a minor contribution to the BM mechanical properties, Collagen IV, which deposition in the BM depends on Laminin (Díaz de la Loza et al., 2017) has a major contribution to these properties, and in particular to its stiffness (Töpfer et al., 2022). Actually, this BM is characterized by a gradient of stiffness, due to a gradient of Collagen IV, endowing the BM with anisotropic resistance to tissue expansion, allowing egg chamber elongation (Crest et al., 2017). Even though the putative loss of mechanical properties leading to OP deformation observed in the *sly* mutant is a consequence of a Laminin loss-of-function, it remains conceivable that it is the Collagen IV, rather than the Laminin itself, which is responsible of these mechanical properties in wild-type animals. This hypothesis, in line with the dramatic disorganization of the Collagen IV pattern observed by immunofluorescence in the *sly* mutant, however requires to be challenged by further investigation.

BMs were for long considered as inert and passive biological material, unable to generate forces by themselves. We now know that their composition is dynamic during morphogenesis (Díaz de la Loza et al., 2017; Harunaga et al., 2014; Khalilgharibi and Mao, 2021; Van De Bor et al., 2021) and this dynamics has been proposed to generate autonomous stresses, i.e. within the BM itself (Loganathan et al., 2016; Pastor-Pareja and Xu, 2011; Zamir et al., 2008). Accordingly,

Serna-Morales et al. (Serna-Morales et al., 2023) recently showed that the *Drosophila* ventral nerve cord morphogenesis is driven by a sudden increase in ECM-driven surface tension due to exponential assembly of Collagen IV in the BM. Still in *Drosophila*, it was recently shown that the elastic ECM enveloping the wing imaginal disc is a form of "active" shell whose anisotropic growth affects the tissue layers upon morphogenesis (Harmansa et al., 2023). Whether such mechanisms participate to the control of the OP shape during the brain flexure remains to be addressed, through the analysis of the dynamics of expression of Collagen IV or other components of the BM as well as biomechanical investigations.

A dramatic consequence of the absence of proper OP and brain BMs in the *sly* mutant is the irregular and undefined frontier between the brain and OP, with placodal cells tending to locally intermingle with brain cells, and vice versa, along the OP/brain interface. This highlights a key role of these BMs in establishing a robust and straight boundary between the OP and the brain. Tissue intermixing has also been observed in the pharynx of Laminin mutants in C. elegans (Huang et al., 2003) and in the Xenopus notochord upon loss-of-function of the Dystroglycan, a major Laminin receptor (Buisson et al., 2014). The absence of a clear boundary between the OP and the brain in the *sly* mutant is accompanied by an apparent distortion of the brain, with notable reduced dimension in its medio-lateral axis. This phenotype, possibly due to the inward migration of the placodes that become partially embedded in the brain, illustrates an additional and unexpected role of the OP and brain BMs, in preventing late convergence of the two placodes towards each other during the flexure movement.

BMs act as cues participating to the pathfinding of olfactory axons along their journey from the OP to the olfactory bulb

The early development of zebrafish olfactory axons begins with their retrograde extension, involving the attachment of the tips of the axonal protrusions to the brain's surface, followed by a lateral movement of the OP cell bodies in the opposite direction (Breau et al., 2017). This initial step appears not to be affected in the *sly* mutant. These results suggest that Laminin-dependent BMs are dispensable for this retrograde axon extension and, more specifically, that Laminin γ1 itself or other components of the BMs are unlikely to play a role in the anchoring of those axon tips onto the brain's surface, which is a prerequisite for their retrograde extension.

Our study shows that following retrograde elongation in the OP, the axons grow and navigate using bona fide growth cones, assemble a tight axon fascicle which crosses the BM of the OP, turns and migrates dorsally for a short distance between both BMs and thereafter crosses the brain BM to navigate towards the olfactory bulb. In other words, the olfactory axons have to cross two BMs. Our data show that the axons cross the first BM as it is still under construction and contain perforations, thus taking advantage of BM-free small pores to exit the OP and reach the narrow area located between the two BMs. By contrast, the entry point into the brain, across the second BM, opens with the arrival of the axons, suggesting that this opening is achieved by the axons themselves. It will be interesting, in future work, to determine whether the axons locally degrade the BM through the secretion of matrix metalloproteases, or displace the BM with protrusive forces, or use a combination of both mechanisms (Chang and Chaudhuri, 2019; Ihara et al., 2011; Nazari et al., 2022; Yamada et al., 2022).

As they migrate in the narrow corridor between the OP and brain BMs, olfactory axons remain confined in close proximity to the Laminin-rich BMs. Entering into the brain tissue, olfactory axons migrate collectively within a dynamic bundle growing towards the presumptive olfactory bulb. Importantly, once they have reached the brain tissue, the distalmost tip of this axon bundle still grows in close apposition to the internal surface of the brain's BM, suggesting that this BM serves as a migratory path promoting the growth of these axons. This hypothesis is reinforced by the fact that axon growth and directionality are dramatically impaired in the *sly* mutant, in which only few axons expressing *Tg(omp:meYFP)* can extend properly towards their target area. This

phenotype is unlikely to be the result of defects in neuronal differentiation, as demonstrated by HuC immunolabeling and expression of the *Tg(neurog1:GFP)* and *Tg(omp:meYFP*) transgenes, which do not show obvious difference as compared to control animals, but appears to be rather due to axon growth and navigation defects. We did not formally identify the component(s) of the BM involved in this axon extension and pathfinding, but we consider Laminin itself as a good candidate for acting as a privileged substrate the axons, as Laminin does so for other populations of axons in zebrafish (Paulus and Halloran, 2006; Semina et al., 2006), and has been shown in rodents to favor OSN axon extension *in vitro*, and to be present *in vivo* along the path followed by OSN axons from the olfactory epithelium to the bulb (Kafitz and Greer, 1997). From a molecular point of view, it has been established on cultured sympathetic neurons that Laminin accelerates the growth of axons through binding to integrins, which favors the formation of F-actin in the growth cone in a microtubule- and Rac1-dependent manner (Grabham et al., 2003). Recently, Abe et al. (2021) further documented another role of Laminin in promoting hippocampal neuron growth cones enhanced progression on stiff substrate, through its interaction with L1, highlighting a new mechanosensitive axon outgrowth mediated by a L1-Laminin clutch mechanism (Abe et al., 2021). Whereas such Laminin-dependent mechanisms are used for guiding olfactory axons in zebrafish remains to be further explored. Other components of the BM, also affected in the *sly* mutant, may be involved as well in the regulation of olfactory axon development. Still in rodents indeed, the characterisation of the expression of ECM proteins along the developing olfactory pathway unraveled a complex interplay between ECM permissive and inhibitory cues expressed in a dynamic way, appearing to restrict axons to the pathway while promoting axon outgrowth within (Shay et al., 2008).

In addition to ECM molecules present in the BMs, guidance cues interacting with these molecules may also be involved in some aspects of the axonal defects observed in the *sly* mutant. For example, while Xenopus retinal axons are repulsed by ephrin-A5 on fibronectin, they are attracted by ephrin-A5 on Laminin (Weinl et al., 2003), and Laminin converts netrin-mediated attraction of these axons to repulsion (Höpker et al., 1999). Moreover, whereas slit2 repulses Robo expressing axons of dorsal root ganglia neurons, this repulsive effect is lost in absence of Laminin (Nguyen-Ba-Charvet et al., 2001). Netrin1a and 1b are expressed in the zebrafish forebrain close to the route of the axons, where they play an attractive role for olfactory axons which express the netrin receptor DCC (Dang et al., 2023; Lakhina et al., 2012). In addition, several ephrin and slits ligands are expressed in the forebrain at stages of axonal growth (*zfin.org*, Miyasaka et al., 2005). We may thus envisage that the absence of Laminin in the *sly* mutant may change in some way the netrin-, ephrin- or slit-dependent pathfinding of olfactory axons.

In conclusion, our findings indicate that the boundary between the sensory and central components of the olfactory system (Suter and Jaworski, 2019) is organised by the BMs of the OP and the brain. These BMs are permeable at specific locations to allow the sensory axons to enter the brain and use them as a substrate to grow towards the olfactory bulb, and at the same time they maintain OP shape and position in the face of major morphogenetic movements occuring during the brain flexure, and ensure proper separation of the two tissues by preventing their intermixing.

Material and methods

Zebrafish lines

Wild-type, transgenic and mutant zebrafish embryos were obtained by natural spawning. In the text, the developmental times in hpf indicate hours post-fertilization at 28°C. To obtain the 14-22 hpf stages, embryos were collected at 10 am, incubated for 2h at 28°C before being placed overnight in a 23°C incubator to slow down development. Using this protocol, the embryos were at 14 hpf in the following morning at 10 am. We used the following lines (the simplified names are

used in the figures and their legends): the zebrafish *sly*^{wi390} (*sly/lamc1*) mutant (referred to as the *sly* mutant, Wiellette et al., 2004), the *foxd3*^{zdf10} mutant (referred to as the *foxd3* mutant, Stewart et al., 2006), *Tg(-8.4neurog1:GFP)*^{sb1} (referred to as *Tg(neurog1:GFP)*, Blader et al., 2003) to label the EONs at coalescence stages, *Tg(-2.0ompb:gapYFP)*^{rw032} (a gift from Nobuhiko Miyasaka, RIKEN Institute, National Bioresource Project of Japan, referred to as *Tg(omp:meYFP)*, Sato et al., 2007) to label *ompb*-expressing OP neurons and their axons from 22 hpf, *Tg(-4.0cldnb:GalTA4, cry:RFP)*^{nim11} (referred to as *Tg(cldnb:Gal4)*, Breau et al., 2013) combined with *Tg(14XUAS:mRFP,Xla.Cryg:GFP)*^{tpl2} (referred to as *Tg(UAS:RFP)*,Balciuniene et al., 2013) to label all cells of the OP and their axons, *TgBAC(lamC1:lamC1-sfGFP)* (Yamaguchi et al., 2022) to visualise the expression of LamC1-sfGFP under the control of the *lamC1* promoter, and *Tg(eltC:GFP)*^{zf199Tg} (referred to as *Tg(elementC:gfp)*,Stedman et al., 2009) to label the forebrain. To generate the *Tg(UAS:lyn-tagRFP)* line, a *10XUAS:lyn-tagRFP* plasmid was synthesized by Gateway cloning (final destination vector: pDest:tol2) and co-injected with Tol2 mRNA (25 ng/µL of plasmid and 25 ng/µL of Tol2 mRNA) in 1 cell-stage wild type embryos. All our experiments were made in agreement with the European Directive 210/63/EU on the protection of animals used for scientific purposes, and the French application decree “Décret 2013-118”. The fish facility has been approved by the French “Service for animal protection and health”, with the approval number B-75-05-25.

Genotyping

The *sly*^{wi390} mutant allele and the wild type locus were genotyped by PCR with the following primers: FW: 5’-CATGACGGCAAAGTTGGTGA-3’; RV1: 5’-CCATGCCTTGCAAAATGGCGTTA CTTAA-3’; RV2: 5’-TGTAGGAGAGAAGTCGCGAG-3’. To detect the *sly*^{wi390} allele (which is an insertion mutant allele, Wiellette et al., 2004), the FW and RV1 were used to amplify a PCR product of 554 bp. The wild type allele was detected with the FW and RV2 primers to amplify a PCR product of 617 bp. The *foxd3*^{zdf10}allele was genotyped with the CAPS (Cleaved Amplified Polymorphic Sequences) technique (Neff et al., 2002) using the SspI restriction enzyme (NEB, R132S), as described in Bryan et al., 2020.

Immunostainings

For Laminin, Nidogen and Collagen IV immunostainings, embryos were fixed in 4% paraformaldehyde (PFA, in PBS), dehydrated in methanol/PBS series and stored in methanol at −20°C. Embryos were rehydrated in methanol/PBS series, washed in PBS and treated with 10 µg/mL proteinase K (embryos at 24 hpf or younger: 1 min 30 s of incubation, later stages: 3 min of incubation). Embryos were then whashed in glycin 2 mg/mL, post-fixed in 4% PFA and washed in PBS. For the other immunostainings, embryos were simply fixed in 4% PFA and washed in PBS. Embryos were then blocked in 3% goat serum and 0.3% triton in PBS for 2h at room temperature or overnight at 4°C and incubated overnight at 4°C with primary and secondary antibodies.

The following primary antibodies were used: anti-Laminin (rabbit, 1/200, L-9393, Sigma), anti-Nidogen (rabbit, 1/200, ab14511, Abcam), anti-Collagen IV (rabbit, 1/200, ab6586, Abcam), anti-GFP (chicken, 1/200, GFP-1020, Aves labs), anti-DsRed (rabbit, 1/300, 632496, Takara), anti-phospho-Histone H3 (rabbit, 1/200, 06-570, Millipore), anti-activated Caspase 3 (rabbit, 1/200, AF835, R and D systems), anti-HuC/D (mouse, 1/200, clone 16A11, A-21271, Thermofischer scientific) and anti-Dlx3b (mouse, 1/500, ZIRC).

In situ hybridisation

Partial cDNA sequences for the NCC *crestin* marker were amplified by PCR using the 5’-AAGCCCTCGAAACTCACCTG-3’ (FW) and 5’-CCACTTGATTCCCACGAGCT-3’ (RV) primers. PCR products were subcloned in pGEM-T-easy (Promega) and sequenced. The Digoxigenin(DIG)-labelled riboprobe was synthetized from PCR templates. Embryos were fixed in 4% PFA in PBS and stored in methanol at − 20 °C. Embryos were then rehydrated in methanol/PBS series,

permeabilized 1 min 30 s with proteinase K (10 mg/ml), pre-hybridized, and hybridized overnight at 65 °C in hybridization mixture (50% formamide, 5 X standard saline citrate (SSC), 0.1% Tween 20, 100 µg/ml heparin, 100 µg/ml tRNA in water). The embryos were subjected to a series of washes in 50% SSC/formamide and SSC/PBST, and were then incubated in the blocking solution (0.2% Tween 20, 0.2% Triton X-100, 2% sheep serum in PBST) for one hour and overnight at 4 °C with alkaline phosphatase-conjugated anti-DIG antibodies (Roche) diluted at 1/4000 in the blocking solution. Embryos were then washed in PBST, soaked in staining buffer (TMN: 0,1M NaCl, 0,1M Tris-HCl, pH 9.5, 0.1% Tween 20 in water) and incubated in NBT/BCIP (nitroblue tetrazolium/5-bromo-4-chloro-3-indolyl phosphate) solution (Roche).

DNA injection

To achieve mosaic labelling, the *-8.4neurog1:GFP* plasmid (Blader et al., 2003), the *omp:meYFP* plasmid (Miyasaka et al., 2005) and the *sox10(7.2):KalTA4* plasmid (Almeida et al., 2015) were injected respectively at 10, 5 and 15 ng/µL in 1-cell stage embryos.

Image acquisition

For live imaging, embryos were dechorionated manually and mounted at 14 hpf in 0.5% low melting agarose in 1X E3 medium. For movies on *Tg(neurog1:GFP)* embryos at coalescence stages, the embryos were imaged directly after the mounting, using a dorsal view, from 14 to 22 hpf (or 14 to 32 hpf for embryos in which NCC were mosaically labelled). For movies on *Tg(omp:meYFP)* embryos, the embryos were placed at 33°C just after the mounting, and imaged from 22 hpf with a frontal view. Movies were recorded at 28°C on a Leica TCS SP8 MPII upright multiphoton microscope using a 25X (numerical aperture (NA) 0.95) water lens. For fixed embryos, immunostained embryos were mounted in 0.5% low melting agarose in PBS and imaged on a Leica TCS SP5 AOBS upright confocal microscope using a 63X (NA 0.9) water lens or on a Zeiss 980 FAST Airyscan with a 20X (NA 1.0) water lens.

For electron microscopy, the zebrafish embryos were fixed in 2% glutaraldehyde and 2% PFA in 0.1M sodium cacodylate buffer pH 7.2 overnight at 4°C. Samples were washed in 0.1M cacodylate buffer, incubated for 1h in 1% osmium tetroxide in 0.1M cacodylate buffer, washed with deionized water, incubated 1h in 1% Uranyl Acetate and washed again with deionized water. To facilitate their orientation for sectionning, the zebrafish embryos were embedded in 4% agarose before being dehydrated through graded concentration of ethanol (50-70-95-100%). Samples were pre-embedded with graded concentration of anhydrous acetone and EPON epoxy resin mix (3:1 – 1:1 – 1:3) and embedded with 100% EPON. Finally, the embryos were mounted on silicon flat mold and polymerized at 60°C for 72 h. Ultrathin sections (80 nm) were prepared with an Ultracut ultramicrotome (UCT, Leica microsystems). They were deposited on silicon wafers, and contrasted with 2.5% uranyl acetate and 2% lead citrate. The wafers were stuck on aluminum stubs, plasma-cleaned, and observed at 1.5 kV, with a 30 µm aperture diameter and high current mode, at 2 mm WD, with SE and BSE in column detectors, in high vacuum in a Field-Emission SEM (Gemini 500, Zeiss). Images were automatically acquired with Atlas 5 (Fibics), with a pixel dwell time of 12.8 µs, a line averaging of 5, with a 8192 x 8192 definition and a pixel size fixed at 2.5 nm (corresponding to an image size of 20.5 × 20.5 µm), and an overlap of 16% between images. To obtain final mosaics, LookUp Table were inverted, SE and BSE signals were mixed, and manual stitching was made.

Image analysis

OP and brain dimensions

The ML dimension of the OP represents the distance between the most medial and the most lateral GFP+ or YFP+ cells in *Tg(neurog1:GFP)* or *Tg(omp:meYFP)* embryos, respectively. Ectopic fluorescent cells (cells that are physically separated from the main cluster) were not taken into

account for this measurement. The same method was applied to quantify the AP and DV dimensions of the OP tissue. The width of the brain was measured along the ML axis using the GFP forebrain expression in *Tg(elementC:gfp)* embryos, at 3 different AP positions and 3 different DV positions.

Thickness of the intercellular space in EM images

Analyses were performed on 1000 pixel-long rectangular regions at the interface between NCC and brain or OP cells in controls, and at the brain/OP interface in *sly* mutants (from 3 to 7 regions per embryo). In each region, the thickness of the intercellular space was manually measured every 100 pixels using Fiji (10 measurements/region). The average thickness per region and then per embryo was computed and plotted.

Manual cell tracking

Individual cells from the OP (expressing *Tg(neurog1:GFP)* or *Tg(omp:meYFP)*) and the adjacent brain were tracked in 3D using the Manual Tracking plugin in ImageJ/Fiji. For tracking on *Tg(neurog1:GFP)* embryos, tracked cells from the brain and the OP expressed *Tg(neurog1:GFP)* at least at the end of the movie. For tracking on *Tg(omp:meYFP)* embryos, we followed forebrain cells located between the two OPs. For growth cone tracking, individual growth cones were followed in 3D using the same plugin in embryos injected with the *omp:meYFP* plasmid, over periods of 200 min each. The orientation of the trajectories represents the angle between the track and the vertical DV axis. 2D color coded trajectories and rose plots were generated in Matlab (Mathworks, US). The 3D MSD was computed using the Numpy library in Python (Harris et al., 2020). Plots representing cell tracks merged at their origin were produced with Microsoft Excel.

Segmentation and analysis of the brain/OP boundary

The segmentation of Dlx3b+ OP cells was performed using a two-step workflow in Ilastik and Fiji softwares. First, to achieve pixel classification, 3 representative images of controls and of *sly* mutants were loaded into the data input menu and used to train the algorithm. After the training the pixel features and feature size (sigma) were selected. All features on all sigma scales were selected. This allowed pixels to be classified based on gray intensity, resemblance to an edge, and texture. Next, the supervised training was performed. 3 examples of each object were labelled; then, the classifier was allowed to update to observe the results. Using the uncertainty overlay, areas of high uncertainty were labeled iteratively until the prediction layer showed satisfactory identification of the pixels. This process was repeated for all 3 images. The trained classifier was then run on all images, and the pixel classification data were saved as segmented images. In the second step, a “region of interest” (ROI) containing the brain/OP boundary was manually defined using Fiji. The edge detection was applied in that ROI and allowed the delineation of the boundary between segmented OP cells and brain cells. The data were exported as CSV files to be used for analysis. The distortion index is defined as the total length of the boundary, divided by the distance between the dorsalmost and ventralmost positions along the analysed boundary region.

Statistical analysis

Most graphs show means ± standard error of the mean (sem), overlayed with all individual data points. These plots were generated with the GraphPad Prism software. For all graphs, we checked for normality of the data distribution before performing parametric, unpaired, two tailed t tests. When the data were not normally distributed, a Mann-Whitney test was used. A Chi2 test was performed on the data presented in Fig. S2M-P and Fig. S4I-L. For the segmentation of the brain/OP boundary (**Fig. 5G, H**), the data were analyzed through an ANOVA test (mixed models, with animals as random effect and genotype and side as fixed effects). The orientation of cell and growth cone trajectories were treated as circular variables and analysed between groups using the

circular analysis of variance based on the likelihood ratio test (**Fig. 4O** and **Fig. 6C, F, I, L**). The p values correspond to *p < 0.05, **p < 0.01, ***p < 0.001. No statistical method was used to estimate sample size and no randomization was performed.

Acknowledgements

We gratefully acknowledge Isabelle Bonnet for her help in image analysis, and Alexis Eschstruth for his help in molecular biology. This work was funded by the Agence Nationale pour la Recherche (ANR-17-CE13-0009-01 NEUROMECHANICS and ANR-23-CE13-0025 MECAMATRIX), the Centre National pour la Recherche Scientifique (CNRS), Sorbonne Université, and the National Institute of Health NIDCD Grant R01-DC-017989. We also thank the imaging platform of the Institut de Biologie Paris-Seine (the facility is supported by CNRS, Sorbonne Université and the Conseil Régional Ile-de-France), and the IBPS aquatic platform for fish care.

References

Abe K., Baba K., Huang L., Wei K. T., Okano K., Hosokawa Y., Inagaki N (2021) **Mechanosensitive axon outgrowth mediated by L1-laminin clutch interface** *Biophys J* **120**:3566–3576

Aguillon R., Madelaine R., Aguirrebengoa M., Guturu H., Link S., Dufourcq P., Lecaudey V., Bejerano G., Blader P., Batut J (2020) **Morphogenesis is transcriptionally coupled to neurogenesis during peripheral olfactory organ development** *Development* **147**

Almeida R.G., Lyons D.A (2015) **Intersectional Gene Expression in Zebrafish Using the Split KalTA4 System** *Zebrafish* **12**:377–86

Anderson C., Thorsteinsdóttir S., Borycki A.G (2009) **Sonic hedgehog-dependent synthesis of laminin alpha1 controls basement membrane assembly in the myotome** *Development* **136**:3495–504

Balciuniene J., Nagelberg D., Walsh K. T., Camerota D., Georlette D., Biemar F., Bellipanni G., Balciunas D (2013) **Efficient disruption of Zebrafish genes using a Gal4-containing gene trap** *BMC Genomics* **14**

Baraban M., Gordillo Pi C., Bonnet I., Gilles J.-F., Lejeune C., Cabrera M., Tep F., Breau M. A (2023) **Actomyosin contractility in olfactory placode neurons opens the skin epithelium to form the zebrafish nostril** *Dev Cell* **58**:361–375

Belvindrah R., Hankel S., Walker J., Patton B. L., Müller U (2007) **Beta1 integrins control the formation of cell chains in the adult rostral migratory stream** *J Neurosci* **27**:2704–2717

Blader P., Plessy C., Strahle U (2003) **Multiple regulatory elements with spatially and temporally distinct activities control neurogenin1 expression in primary neurons of the zebrafish embryo** *Mech Dev* **120**:211–8

Bonner J., O'Connor T. P (2001) **The permissive cue laminin is essential for growth cone turning in vivo** *J Neurosci* **21**:9782–9791

Breau M. A., Wilkinson D. G., Xu Q (2013) **A Hox gene controls lateral line cell migration by regulating chemokine receptor expression downstream of Wnt signaling** *Proc Natl Acad Sci U S A* **110**:16892–16897

Breau M. A., Bonnet I., Stoufflet J., Xie J., De Castro S., Schneider-Maunoury S. (2017) **Extrinsic mechanical forces mediate retrograde axon extension in a developing neuronal circuit** *Nat Commun* **8**

Breau M. A., Trembleau A (2023) **Chemical and mechanical control of axon fasciculation and defasciculation** *Semin Cell Dev Biol* **140**:72–81

Bryan C. D., Chien C. B., Kwan K. M (2016) **Loss of laminin alpha 1 results in multiple structural defects and divergent effects on adhesion during vertebrate optic cup morphogenesis** *Dev Biol* **416**:324–37

Bryan C. D., Casey M. A., Pfeiffer R. L., Jones B. W., Kwan K. M (2020) **Optic cup morphogenesis requires neural crest-mediated basement membrane assembly** *Development* **147**

Buisson N., Sirour C., Moreau N., Denker E., Le Bouffant R., Goullancourt A., Darribère T., Bello V. (2014) **An adhesome comprising laminin, dystroglycan and myosin IIA is required during notochord development in Xenopus laevis** *Development* **141**:4569–79

Chang J., Chaudhuri O (2019) **Beyond proteases: Basement membrane mechanics and cancer invasion** *J Cell Biol* **218**:2456–2469

Chapman S. C., Sawitzke A. L., Campbell D. S., Schoenwolf G. C (2005) **A three-dimensional atlas of pituitary gland development in the zebrafish** *J Comp Neurol* **487**:428–440

Chen Z.-L., Haegeli V., Yu H., Strickland S. (2009) **Cortical deficiency of laminin gamma1 impairs the AKT/GSK-3beta signaling pathway and leads to defects in neurite outgrowth and neuronal migration** *Dev Biol* **327**:158–168

Crest J., Diz-Muñoz A., Chen D. Y., Fletcher D. A., Bilder D (2017) **Organ sculpting by patterned extracellular matrix stiffness** *Elife* **6**

Dang P., Barnes D. T., Cheng R. P., Xu A., Moon Y. J., Kodukula S. S., Raper J. A (2023) **Netrins and Netrin Receptors are Essential for Normal Targeting of Sensory Axons in the Zebrafish Olfactory Bulb** *Neuroscience* **508**:19–29

Díaz de la Loza M. C., Díaz-Torres A., Zurita F., Rosales-Nieves A. E., Moeendarbary E., Franze K., Martín-Bermudo M. D., González-Reyes A. (2017) **Laminin Levels Regulate Tissue Migration and Anterior-Posterior Polarity during Egg Morphogenesis in Drosophila** *Cell Rep* **20**:211–223

Dolez M., Nicolas J.-F., Hirsinger E (2011) **Laminins, via heparan sulfate proteoglycans, participate in zebrafish myotome morphogenesis by modulating the pattern of Bmp responsiveness** *Development* **138**:97–106

Dynes J. L., Ngai J (1998) **Pathfinding of olfactory neuron axons to stereotyped glomerular targets revealed by dynamic imaging in living zebrafish embryos** *Neuron* **20**:1081–1091

Garcia K. E., Okamoto R. J., Bayly P. V., Taber L. A (2017) **Contraction and stress-dependent growth shape the forebrain of the early chicken embryo** *J Mech Behav Biomed Mater* **65**:383–397

García-Alonso L., Fetter R. D., Goodman C. S (1996) **Genetic analysis of Laminin A in Drosophila: extracellular matrix containing laminin A is required for ocellar axon pathfinding** *Development* **122**:2611–2621

Grabham P. W., Reznik B., Goldberg D. J (2003) **Microtubule and Rac 1-dependent F-actin in growth cones** *J Cell Sci* **116**:3739–3748

Grant P. K., Moens C. B (2010) **The neuroepithelial basement membrane serves as a boundary and a substrate for neuron migration in the zebrafish hindbrain** *Neural Dev* **5**

Harden M. V., Pereiro L., Ramialison M., Wittbrodt J., Prasad M. K., McCallion A. S., Whitlock K. E (2012) **Close association of olfactory placode precursors and cranial neural crest cells does not predestine cell mixing** *Dev Dyn* **241**:1143–54

Harmansa S., Erlich A., Eloy C., Zurlo G., Lecuit T (2023) **Growth anisotropy of the extracellular matrix shapes a developing organ** *Nat Commun* **14**

Harris C. R. *et al.* (2020) **Array programming with NumPy** *Nature* **585**:357–362

Harunaga J. S., Doyle A. D., Yamada K. M (2014) **Local and global dynamics of the basement membrane during branching morphogenesis require protease activity and actomyosin contractility** *Dev Biol* **394**:197–205

Hauptmann G., Gerster T (2000) **Regulatory gene expression patterns reveal transverse and longitudinal subdivisions of the embryonic zebrafish forebrain** *Mech Dev* **91**:105–118

Höpker V. H., Shewan D., Tessier-Lavigne M., Poo M., Holt C (1999) **Growth-cone attraction to netrin-1 is converted to repulsion by laminin-1** *Nature* **401**:69–73

Huang C.-C., Hall D. H., Hedgecock E. M., Kao G., Karantza V., Vogel B. E., Hutter H., Chisholm A. D., Yurchenco P. D., Wadsworth W. G (2003) **Laminin alpha subunits and their role in C. elegans development** *Development* **130**:3343–3358

Ihara S., Hagedorn E. J., Morrissey M. A., Chi Q., Motegi F., Kramer J. M., Sherwood D. R (2011) **Basement membrane sliding and targeted adhesion remodels tissue boundaries during uterine-vulval attachment in Caenorhabditis elegans** *Nat Cell Biol* **13**:641–651

Ivanovitch K., Cavodeassi F., Wilson S. W (2013) **Precocious acquisition of neuroepithelial character in the eye field underlies the onset of eye morphogenesis** *Dev Cell* **27**:293–305

Kafitz K. W., Greer C. A (1997) **Role of laminin in axonal extension from olfactory receptor cells** *J Neurobiol* **32**:298–310

Karamanos N. K., Piperigkou Z., Passi A., Götte M., Rousselle P., Vlodavsky I (2021) **Extracellular matrix-based cancer targeting** *Trends Mol Med* **27**:1000–1013

Karlstrom R. O. *et al.* (1996) **Zebrafish mutations affecting retinotectal axon pathfinding** *Development* **123**:427–438

Kaur S., Kaur I., Rawal P., Tripathi D. M., Vasudevan A (2021) **Non-matrigel scaffolds for organoid cultures** *Cancer Lett* **504**:58–66

Khalilgharibi N., Mao Y (2021) **To form and function: on the role of basement membrane mechanics in tissue development, homeostasis and disease** *Open Biol* **11**

Kim S., Uroz M., Bays J. L., Chen C. S (2021) **Harnessing Mechanobiology for Tissue Engineering** *Dev Cell* **56**:180–191

Lakhina V., Marcaccio C. L., Shao X., Lush M. E., Jain R. A., Fujimoto E., Bonkowsky J. L., Granato M., Raper J. A (2012) **Netrin/DCC signaling guides olfactory sensory axons to their correct location in the olfactory bulb** *J Neurosci* **32**:4440–4456

Lee J., Gross J. M (2007) **Laminin beta1 and gamma1 containing laminins are essential for basement membrane integrity in the zebrafish eye** *Invest Ophthalmol Vis Sci* **48**:2483–2490

Li S., Liquari P., McKee K. K., Harrison D., Patel R., Lee S., Yurchenco P. D (2005) **Laminin-sulfatide binding initiates basement membrane assembly and enables receptor signaling in Schwann cells and fibroblasts** *J Cell Biol* **169**:179–189

Loganathan R., Rongish B. J., Smith C. M., Filla M. B., Czirok A., Bénazéraf B., Little C. D (2016) **Extracellular matrix motion and early morphogenesis** *Development* **143**:2056–2065

Luo R., An M., Arduini B. L., Henion P. D (2001) **Specific pan-neural crest expression of zebrafish Crestin throughout embryonic development** *Dev Dyn* **220**:69–74

Madelaine R., Garric L., Blader P (2011) **Partially redundant proneural function reveals the importance of timing during zebrafish olfactory neurogenesis** *Development* **138**:4753–62

Miner J. H., Yurchenco P. D (2004) **Laminin functions in tissue morphogenesis** *Annu Rev Cell Dev Biol* **20**:255–284

Miyasaka N., Sato Y., Yeo S.-Y., Hutson L. D., Chien C.-B., Okamoto H., Yoshihara Y (2005) **Robo2 is required for establishment of a precise glomerular map in the zebrafish olfactory system** *Development* **132**:1283–1293

Miyasaka N., Knaut H., Yoshihara Y (2007) **Cxcl12/Cxcr4 chemokine signaling is required for placode assembly and sensory axon pathfinding in the zebrafish olfactory system** *Development* **134**:2459–2468

Monnot P., Gangatharan G., Baraban M., Pottin K., Cabrera M., Bonnet I, Breau M. A. (2022) **Intertissue mechanical interactions shape the olfactory circuit in zebrafish** *EMBO Rep* **23**

Moore R. E., Pop S., Alleyne C., Clarke J. D. W (2022) **Microtubules are not required to generate a nascent axon in embryonic spinal neurons in vivo** *EMBO reports* **23**

Nazari S. S., Doyle A. D., Yamada K. M (2022) **Mechanisms of Basement Membrane Micro-Perforation during Cancer Cell Invasion into a 3D Collagen Gel** *Gels* **8**

Neff M. M., Turk E., Kalishman M (2002) **Web-based primer design for single nucleotide polymorphism analysis** *Trends Genet* **18**:613–615

Nguyen-Ba-Charvet K. T., Brose K., Marillat V., Sotelo C., Tessier-Lavigne M., Chédotal A (2001) **Sensory axon response to substrate-bound Slit2 is modulated by laminin and cyclic GMP** *Mol Cell Neurosci* **17**:1048–1058

Odenthal J. *et al.* (1996) **Mutations affecting the formation of the notochord in the zebrafish, Danio rerio** *Development* **123**:103–115

Parsons M. J., Pollard S. M., Saúde L., Feldman B., Coutinho P., Hirst E. M. A., Stemple D. L (2002) **Zebrafish mutants identify an essential role for laminins in notochord formation** *Development* **129**:3137–3146

Pastor-Pareja J. C., Xu T (2011) **Shaping Cells and Organs in Drosophila by Opposing Roles of Fat Body-Secreted Collagen IV and Perlecan** *Developmental Cell* **21**:245–256

Paulus J. D., Halloran M. C (2006) **Zebrafish bashful/laminin-alpha 1 mutants exhibit multiple axon guidance defects** *Dev Dyn* **235**:213–224

Pollard S. M., Parsons M. J., Kamei M., Kettleborough R. N. W., Thomas K. A., Pham V. N., Bae M.-K., Scott A., Weinstein B. M., Stemple D. L (2006) **Essential and overlapping roles for laminin alpha chains in notochord and blood vessel formation** *Dev Biol* **289**:64–76

Powell S. K., Kleinman H. K (1997) **Neuronal laminins and their cellular receptors** *Int J Biochem Cell Biol* **29**:401–414

Randlett O., Poggi L., Zolessi F. R., Harris W. A (2011) **The oriented emergence of axons from retinal ganglion cells is directed by laminin contact in vivo** *Neuron* **70**:266–280

Ross L. S., Parrett T., Easter S. S (1992) **Axonogenesis and morphogenesis in the embryonic zebrafish brain** *J Neurosci* **12**:467–482

Sato Y., Miyasaka N., Yoshihara Y (2005) **Mutually exclusive glomerular innervation by two distinct types of olfactory sensory neurons revealed in transgenic zebrafish** *J Neurosci* **25**:4889–4897

Sato Y., Miyasaka N., Yoshihara Y (2007) **Hierarchical regulation of odorant receptor gene choice and subsequent axonal projection of olfactory sensory neurons in zebrafish** *J Neurosci* **27**:1606–1615

Semina E. V., Bosenko D. V., Zinkevich N. C., Soules K. A., Hyde D. R., Vihtelic T. S., Willer G. B., Gregg R. G., Link B. A (2006) **Mutations in laminin alpha 1 result in complex, lens-independent ocular phenotypes in zebrafish** *Dev Biol* **299**:63–77

Serna-Morales E. *et al.* (2023) **Extracellular matrix assembly stress initiates Drosophila central nervous system morphogenesis** *Dev Cell* **58**:825–835

Shay E. L., Greer C. A., Treloar H. B (2008) **Dynamic expression patterns of ECM molecules in the developing mouse olfactory pathway** *Dev Dyn* **237**:1837–1850

Sidhaye J., Norden C (2017) **Concerted action of neuroepithelial basal shrinkage and active epithelial migration ensures efficient optic cup morphogenesis** *Elife* **6**

Sittaramane V., Sawant A., Wolman M. A., Maves L., Halloran M. C., Chandrasekhar A (2009) **The cell adhesion molecule Tag1, transmembrane protein Stbm/Vangl2, and Lamininalpha1 exhibit genetic interactions during migration of facial branchiomotor neurons in zebrafish** *Dev Biol* **325**:363–373

Smyth N., Vatansever H. S., Murray P., Meyer M., Frie C., Paulsson M., Edgar D (1999) **Absence of basement membranes after targeting the LAMC1 gene results in embryonic lethality due to failure of endoderm differentiation** *J Cell Biol* **144**:151–160

Soleman S., Filippov M. A., Dityatev A., Fawcett J. W (2013) **Targeting the neural extracellular matrix in neurological disorders** *Neuroscience* **253**:194–213

Stedman A., Lecaudey V., Havis E., Anselme I., Wassef M., Gilardi-Hebenstreit P., Schneider-Maunoury S (2009) **A functional interaction between Irx and Meis patterns the anterior hindbrain and activates krox20 expression in rhombomere 3** *Dev Biol* **327**:566–577

Stemple D. L. *et al.* (1996) **Mutations affecting development of the notochord in zebrafish** *Development* **123**:117–128

Stewart R. A., Arduini B. L., Berghmans S., George R. E., Kanki J. P., Henion P. D., Look A. T (2006) **Zebrafish foxd3 is selectively required for neural crest specification, migration and survival** *Developmental Biology* **292**:174–188

Suter T., Jaworski A (2019) **Cell migration and axon guidance at the border between central and peripheral nervous system** *Science* **365**

Theocharis A. D., Manou D., Karamanos N. K (2019) **The extracellular matrix as a multitasking player in disease** *FEBS J* **286**:2830–2869

Töpfer U., Guerra Santillán K. Y., Fischer-Friedrich E., Dahmann C (2022) **Distinct contributions of ECM proteins to basement membrane mechanical properties in Drosophila** *Development* **149**

Torres-Paz J., Whitlock K. E (2014) **Olfactory sensory system develops from coordinated movements within the neural plate** *Dev Dyn* **243**:1619–31

Torres-Paz J., Tine E. M., Whitlock K. E (2021) **Dissecting the neural divide: a continuous neurectoderm gives rise to the olfactory placode and bulb** *Int J Dev Biol* **65**:275–287

Tropepe V., Sive H. L (2003) **Can zebrafish be used as a model to study the neurodevelopmental causes of autism?** *Genes Brain Behav* **2**:268–281

Tsuda S. *et al.* (2010) **FAK-mediated extracellular signals are essential for interkinetic nuclear migration and planar divisions in the neuroepithelium** *J Cell Sci* **123**:484–496

Urbano J. M., Torgler C. N., Molnar C., Tepass U., López-Varea A., Brown N. H., de Celis J. F., Martín-Bermudo M. D. (2009) **Drosophila laminins act as key regulators of basement membrane assembly and morphogenesis** *Development* **136**:4165–4176

Van De Bor V., Loreau V., Malbouyres M., Cerezo D., Placenti A., Ruggiero F., Noselli S. (2021) **A dynamic and mosaic basement membrane controls cell intercalation in Drosophila ovaries** *Development* **148**

Vöcking O., Van Der Meulen K., Patel M. K., Famulski J. K. (2023) **Zebrafish anterior segment mesenchyme progenitors are defined by function of tfap2a but not sox10** *Differentiation* **130**:32–42

Walma D. A. C., Yamada K. M (2020) **The extracellular matrix in development** *Development* **147**

Weinl C., Drescher U., Lang S., Bonhoeffer F., Löschinger J (2003) **On the turning of Xenopus retinal axons induced by ephrin-A5** *Development* **130**:1635–1643

Whitlock K. E., Westerfield M (1998) **A transient population of neurons pioneers the olfactory pathway in the zebrafish** *J Neurosci* **18**:8919–8927

Whitlock K. E., Westerfield M (2000) **The olfactory placodes of the zebrafish form by convergence of cellular fields at the edge of the neural plate** *Development* **127**:3645–53

Wiellette E., Grinblat Y., Austen M., Hirsinger E., Amsterdam A., Walker C., Westerfield M., Sive H (2004) **Combined haploid and insertional mutation screen in the zebrafish** *Genesis* **40**:231–240

Wolman M. A., Sittaramane V. K., Essner J. J., Yost H. J., Chandrasekhar A., Halloran M. C (2008) **Transient axonal glycoprotein-1 (TAG-1) and laminin-alpha1 regulate dynamic growth cone behaviors and initial axon direction in vivo** *Neural Dev* **3**

Yamada K. M., Doyle A. D., Lu J (2022) **Cell-3D matrix interactions: recent advances and opportunities** *Trends Cell Biol* **32**:883–895

Yamaguchi N., Zhang Z., Schneider T., Wang B., Panozzo D., Knaut H (2022) **Rear traction forces drive adherent tissue migration in vivo** *Nat Cell Biol* **24**:194–204

Zamir E. A., Rongish B. J., Little C. D (2008) **The ECM moves during primitive streak formation--computation of ECM versus cellular motion** *PLoS Biol* **6**

Author information

Pénélope Tignard
Sorbonne Université, Centre National de la Recherche Scientifique (CNRS UMR7622), Institut de Biologie Paris-Seine (IBPS), Developmental Biology Laboratory, Paris, France, Sorbonne Université, Centre National de la Recherche Scientifique (CNRS UMR8246), Inserm U1130, Institut de Biologie Paris Seine (IBPS), Neuroscience Paris Seine (NPS), Paris, France

Karen Pottin
Sorbonne Université, Centre National de la Recherche Scientifique (CNRS UMR7622), Institut de Biologie Paris-Seine (IBPS), Developmental Biology Laboratory, Paris, France
ORCID iD: 0000-0001-9491-4660

Audrey Geeverding
Imaging Facility, Institut de Biologie Paris-Seine (IBPS), Paris, France
ORCID iD: 0000-0002-0208-0302

Mohamed Doulazmi
Sorbonne Université, Centre National de la Recherche Scientifique (CNRS UMR8256), Institut de Biologie Paris Seine (IBPS), Adaptation Biologique et Vieillissement, Paris, France
ORCID iD: 0000-0002-0313-1490

Mélody Cabrera
Sorbonne Université, Centre National de la Recherche Scientifique (CNRS UMR7622), Institut de Biologie Paris-Seine (IBPS), Developmental Biology Laboratory, Paris, France
ORCID iD: 0000-0002-2310-6284

Coralie Fouquet
Sorbonne Université, Centre National de la Recherche Scientifique (CNRS UMR8246), Inserm U1130, Institut de Biologie Paris Seine (IBPS), Neuroscience Paris Seine (NPS), Paris, France

Mathilde Liffran
Sorbonne Université, Centre National de la Recherche Scientifique (CNRS UMR8246), Inserm U1130, Institut de Biologie Paris Seine (IBPS), Neuroscience Paris Seine (NPS), Paris, France

Jonathan Fouchard
Sorbonne Université, Centre National de la Recherche Scientifique (CNRS UMR7622), Institut de Biologie Paris-Seine (IBPS), Developmental Biology Laboratory, Paris, France
ORCID iD: 0000-0002-9976-462X

Marion Rosello
Sorbonne Université, INSERM, CNRS, Institut de la Vision, Paris, France
ORCID iD: 0000-0003-3935-6971

Shahad Albadri
Sorbonne Université, INSERM, CNRS, Institut de la Vision, Paris, France
ORCID iD: 0000-0002-3243-7018

Filippo Del Bene
Sorbonne Université, INSERM, CNRS, Institut de la Vision, Paris, France
ORCID iD: 0000-0001-8551-2846

Alain Trembleau
Sorbonne Université, Centre National de la Recherche Scientifique (CNRS UMR8246), Inserm U1130, Institut de Biologie Paris Seine (IBPS), Neuroscience Paris Seine (NPS), Paris, France
ORCID iD: 0000-0002-8290-0795

For correspondence: alain.trembleau@sorbonne-universite.fr

Marie A Breau
Sorbonne Université, Centre National de la Recherche Scientifique (CNRS UMR7622), Institut de Biologie Paris-Seine (IBPS), Developmental Biology Laboratory, Paris, France, Institut National de la Santé et de la Recherche Médicale (INSERM), Paris, France
ORCID iD: 0000-0003-1884-7704

For correspondence: marie.breau@sorbonne-universite.fr

Editors

Reviewing Editor
Emily Noël
University of Sheffield, Sheffield, United Kingdom

Senior Editor
Didier Stainier
Max Planck Institute for Heart and Lung Research, Bad Nauheim, Germany

Reviewer #1 (Public review):

The authors describe the dynamic distribution of laminin γ1 in the olfactory system and forebrain. Using immunohistochemistry and transgenic lines, they found that the olfactory system and adjacent brain tissues are enveloped by basement membrane (BMs) from the earliest stages of olfactory system assembly. They also found that laminin deposits follow the axonal trajectory of axons. They performed a functional analysis of the sly mutant to analyse the function of laminin γ1 in the development of the zebrafish olfactory system. Their study revealed that laminin enables the shape and position of olfactory placodes to be maintained late in the face of major morphogenetic movements in the brain, and its absence promotes the local entry of sensory axons into the brain and their navigation towards the olfactory bulb.

They showed that in the laminin γ1 mutants no BM staining of laminin could be detected around the OP and the brain. The authors then elegantly used electron microscopy to analyse

the ultrastructure of the border between the OP and the brain.
The authors performed a quantitative analysis of the loss of function of Laminin γ1 (sly mutants).
Olfactory axon migration is drastically impaired in sly mutants, demonstrating that Laminin γ1-dependent BMs are essential for the growth and navigation of axons from the OP to the olfactory bulb. They propose that the BM of the OP prevents its deformation in response to mechanical forces generated by morphogenetic movements of the neighbouring brain.
Although the results are expected, the experiments carried out and the results are robust and elegant.

https://doi.org/10.7554/eLife.92004.2.sa3

Reviewer #2 (Public review):

Summary:

This manuscript addresses the role of extracellular matrix in olfactory development. Despite the importance of these extracellular structures, the specific roles and activities of matrix molecules are still poorly understood. Here, the authors combine live imaging and genetics to examine the role of the laminin gamma 1 in multiple steps of olfactory development. The work comprises a descriptive but carefully executed, quantitative assessment of the olfactory phenotypes resulting from loss of laminin gamma 1. Overall, this is a constructive advance in our understanding of extracellular matrix contributions to olfactory development, with a well-written Discussion with relevance to many other systems.

Strengths:

The strengths of the manuscript are in the approaches: the authors have combined live imaging, careful quantitative analyses, and molecular genetics. The work presented takes advantage of many zebrafish tools including mutants and transgenics to directly visualize the laminin extracellular matrix in living embryos during the developmental process.

Weaknesses:

Weaknesses in the first round of critique were addressed in the revision, and a minor caveat is regarding interpretation of differences in tissue size and shape in fixed samples (comparing mutants and controls); the fixation process can alter these properties and may do so differently between genotypes.

https://doi.org/10.7554/eLife.92004.2.sa2

Reviewer #4 (Public review):

Summary:

In this elegant study XX and colleagues use a combination of fixed tissue analyses and live imaging to characterise the role of Laminin in olfactory placode development and neuronal pathfinding in the zebrafish embryo. They describe Laminin dynamics in the developing olfactory placode and adjacent brain structures and identify potential roles for Laminin in facilitating neuronal pathfinding from the olfactory placode to the brain. To test whether Laminin is required for olfactory placode neuronal pathfinding they analyse olfactory system development in a well-established laminin-gamma-1 mutant, in which the laminin-rich basement membrane is disrupted. They show that while the OP still coalesces in the absence of Laminin, Laminin is required to contain OP cells during forebrain flexure during development and maintain separation of the OP and adjacent brain region. They further

demonstrate that Laminin is required for growth of OP neurons from the OP-brain interface towards the olfactory bulb. The authors also present data describing that while the Laminin mutant has partial defects in neural crest cell migration towards the developing OP, these NCC defects are unlikely to be the cause of the neuronal pathfinding defects upon loss of Laminin. Altogether the study is extremely well carried out, with careful analysis of high-quality data. Their findings are likely to be of interest to those working on olfactory system development, or with an interest in extracellular matrix in organ morphogenesis, cell migration, and axonal pathfinding.

Strengths:

The authors describe for the first time Laminin dynamics during the early development of the olfactory placode and olfactory axon extension. They use an appropriate model to perturb the system (lamc1 zebrafish mutant), and demonstrate novel requirements for Laminin in pathfinding of OP neurons towards the olfactory bulb.
The study utilises careful and impressive live imaging to draw most of its conclusions, really drawing upon the strengths of the zebrafish model to investigate the role of laminin in OP pathfinding. This imaging is combined with deep learning methodology to characterise and describe phenotypes in their Laminin-perturbed models, along with detailed quantifications of cell behaviours, together providing a relatively complete picture of the impact of loss of Laminin on OP development.

Weaknesses:

Some of the statistical tests are performed on experiments where n=2 for each condition (for example the measurements in Figure S2) - in places the data is non-significant, but clear trends are observed, and one wonders whether some experiments are under-powered.

https://doi.org/10.7554/eLife.92004.2.sa1

Author response:

The following is the authors' response to the current reviews.

We are grateful to the reviewers for their positive assessment of the revised version of the article.

Please find below our answers to the last, minor comments of the reviewers.

We thank the reviewer for this important comment. In our live imaging experiments, we actually tracked the dorsal and ventral borders of the omp:yfp positive clusters in control and sly mutant embryos. These measurements showed that the omp:yfp positive clusters are more elongated along the DV axis in mutants as compared with control siblings, as seen on fixed samples (data not shown), suggesting that this difference in tissue shape is not due to fixation.

> ***Reviewer #4 (Public review):***
>
> *Summary:*
>
> *In this elegant study XX and colleagues use a combination of fixed tissue analyses and live imaging to characterise the role of Laminin in olfactory placode development and neuronal pathfinding in the zebrafish embryo. They describe Laminin dynamics in the developing olfactory placode and adjacent brain structures and identify potential roles for Laminin in facilitating neuronal pathfinding from the olfactory placode to the brain. To test whether Laminin is required for olfactory placode neuronal pathfinding they*

> *analyse olfactory system development in a well-established laminin-gamma-1 mutant, in which the laminin-rich basement membrane is disrupted. They show that while the OP still coalesces in the absence of Laminin, Laminin is required to contain OP cells during forebrain flexure during development and maintain separation of the OP and adjacent brain region. They further demonstrate that Laminin is required for growth of OP neurons from the OP-brain interface towards the olfactory bulb. The authors also present data describing that while the Laminin mutant has partial defects in neural crest cell migration towards the developing OP, these NCC defects are unlikely to be the cause of the neuronal pathfinding defects upon loss of Laminin. Altogether the study is extremely well carried out, with careful analysis of high-quality data. Their findings are likely to be of interest to those working on olfactory system development, or with an interest in extracellular matrix in organ morphogenesis, cell migration, and axonal pathfinding.*
>
> *Strengths:*
>
> *The authors describe for the first time Laminin dynamics during the early development of the olfactory placode and olfactory axon extension. They use an appropriate model to perturb the system (lamc1 zebrafish mutant), and demonstrate novel requirements for Laminin in pathfinding of OP neurons towards the olfactory bulb.*
>
> *The study utilises careful and impressive live imaging to draw most of its conclusions, really drawing upon the strengths of the zebrafish model to investigate the role of laminin in OP pathfinding. This imaging is combined with deep learning methodology to characterise and describe phenotypes in their Laminin-perturbed models, along with detailed quantifications of cell behaviours, together providing a relatively complete picture of the impact of loss of Laminin on OP development.*
>
> *Weaknesses:*
>
> *Some of the statistical tests are performed on experiments where n=2 for each condition (for example the measurements in Figure S2) - in places the data is non-significant, but clear trends are observed, and one wonders whether some experiments are under-powered.*

We initially planned the electron microscopy experiments in order to analyse 3 embryos per genotype per stage. However, because of technical issues we could not perform the measurements in all the cases, explaining why we have n = 2 in some of the graphs. The trends were quite clear, so we chose to keep these data in the article. We believe they nicely complement the immunostaining data assessing basement membrane integrity in control and mutant embryos.

The following is the authors' response to the original reviews.

> ***Public Reviews:***
>
> ***Reviewer #1 (Public Review):***
>
> *Summary:*
>
> *The authors describe the dynamic distribution of laminin in the olfactory system and forebrain. Using immunohistochemistry and transgenic lines, they found that the olfactory system and adjacent brain tissues are enveloped by BMs from the earliest stages of olfactory system assembly. They also found that laminin deposits follow the axonal trajectory of axons. They performed a functional analysis of the sly mutant to analyse the function of laminin γ1 in the development of the zebrafish olfactory system.*

Their study revealed that laminin enables the shape and position of placodes to be maintained late in the face of major morphogenetic movements in the brain, and its absence promotes the local entry of sensory axons into the brain and their navigation towards the olfactory bulb.

Strengths:

- They showed that in the sly mutants, no BM staining of laminin and Nidogen could be detected around the OP and the brain. The authors then elegantly used electron microscopy to analyse the ultrastructure of the border between the OP and the brain in control and sly mutant conditions.

- To analyse the role of laminin γ1-dependent BMs in OP coalescence, the authors used the cluster size of Tg(neurog1:GFP)+ OP cells at 22 hpf as a marker. They found that the mediolateral dimension increased specifically in the mutants. However, proliferation did not seem to be affected, although apoptosis appeared to increase slightly at a later stage. This increase could therefore be due to a dispersal of cells in the OP. To test this hypothesis, the authors then analysed the cell trajectories and extracted 3D mean square displacements (MSD), a measure of the volume explored by a cell in a given period of time. Their conclusion indicates that although brain cell movements are increased in the absence of BM during coalescence phases, overall OP cell movements occur within normal parameters and allow OPs to condense into compact neuronal clusters in sly mutants. The authors also analysed the dimensions of the clusters composed of OMP+ neurons. Their results show an increase in cluster size along the dorso-ventral axis. These results were to be expected since, compared with BM, early neurog1+ neurons should compact along the medio-lateral axis, and those that are OMP+ essentially along the dorso-ventral axis. In addition to the DV elongation of OP tissue, the authors show the existence of isolated and ectopic (misplaced) YFP+ cells in sly mutants.

- To understand the origin of these phenotypes, the authors analysed the dynamic behaviour of brain cells and OPs during forebrain flexion. The authors then quantitatively measured brain versus OPs in the sly mutant and found that the OP-brain boundary was poorly defined in the sly mutant compared with the control. Once again, the methods (cell tracks, brain size, and proliferation/apoptosis, and the shape of the brain/OP boundary) are elegant but the results were expected.

- They then analysed the dynamic behaviour of the axon using live imaging. Thus, olfactory axon migration is drastically impaired in sly mutants, demonstrating that Laminin γ1dependent BMs are essential for the growth and navigation of axons from the OP to the olfactory bulb.

- The authors therefore performed a quantitative analysis of the loss of function of Laminin γ1. They propose that the BM of the OP prevents its deformation in response to mechanical forces generated by morphogenetic movements of the neighbouring brain.

Weaknesses:

- The authors did not analyse neurog1 + axonal migration at the level of the single cell and instead made a global analysis. An analysis at the cell level would strengthen their hypotheses.

- Rescue experiments by locally inducing Laminin expression would have strengthened the paper.

- The paper lacks clarity between the two neuronal populations described (early EONs and late OSNs).

> *- The authors quantitatively measured brain versus OPs in the sly mutant and found that the OP-brain boundary was poorly defined in the sly mutant compared with the control. Once again, the methods (cell tracks, brain size, proliferation/apoptosis, and the shape of the brain/OP boundary) are elegant but the results were expected.*
>
> *- A missing point in the paper is the effect of Laminin γ1 on the migration of cranial NCCs that interact with OP cells. The authors could have analysed the dynamic distribution of neural crest cells in the sly mutant.*

We thank the reviewer for the overall positive assessment of our work, and we carefully responded to all her/his insightful comments below. Live imaging experiments to (1) visualise exit and entry point formation with only a few axons labelled, (2) characterise the behaviour of single neurog1:GFP-positive neurons/axons during OP coalescence and to (3) analyse the migration of cranial NCC are now included in the revised manuscript to address the reviewer's questions, and reinforce our initial conclusions.

> ***Reviewer #2 (Public Review):***
>
> *Summary:*
>
> *This manuscript addresses the role of the extracellular matrix in olfactory development. Despite the importance of these extracellular structures, the specific roles and activities of matrix molecules are still poorly understood. Here, the authors combine live imaging and genetics to examine the role of laminin gamma 1 in multiple steps of olfactory development. The work comprises a descriptive but carefully executed, quantitative assessment of the olfactory phenotypes resulting from loss of laminin gamma. Overall, this is a constructive advance in our understanding of extracellular matrix contributions to olfactory development, with a well-written Discussion with relevance to many other systems.*
>
> *Strengths:*
>
> *The strengths of the manuscript are in the approaches: the authors have combined live imaging, careful quantitative analyses, and molecular genetics. The work presented takes advantage of many zebrafish tools including mutants and transgenics to directly visualize the laminin extracellular matrix in living embryos during the developmental process.*
>
> *Weaknesses:*
>
> *The weaknesses are primarily in the presentation of some of the imaging data. In certain cases, it was not straightforward to evaluate the authors' interpretations and conclusions based on the single confocal sections included in the manuscript. For example, it was difficult to assess the authors' interpretation of when and how laminin openings arise around the olfactory placode and brain during olfactory axon guidance.*

We thank the reviewer for the overall positive assessment of our work, and we carefully responded to all her/his insightful comments below. To address these comments, live imaging data to visualise exit and entry point formation with a sparse labelling of axons, and z-stacks showing how exit and entry points are organised in 3D, have been added to the revised manuscript.

> ***Reviewer #3 (Public Review):***
>
> *This is a beautifully presented paper combining live imaging and analysis of mutant phenotypes to elucidate the role of laminin γ1-dependent basement membranes in the*

> *development of the zebrafish olfactory placode. The work is clearly illustrated and carefully quantified throughout. There are some very interesting observations based on the analysis of wild-type, laminin γ1, and foxd3 mutant embryos. The authors demonstrate the importance of a Laminin γ1-dependent basement membrane in olfactory placode morphogenesis, and in establishing and maintaining both boundaries and neuronal connections between the brain and the olfactory system. There are some very interesting observations, including the identification of different mechanisms for axons to cross basement membranes, either by taking advantage of incompletely formed membranes at early stages, or by actively perforating the membrane at later ones.*
>
> *This is a valuable and important study but remains quite descriptive. In some cases, hypotheses for mechanisms are stated but are not tested further. For example, the authors propose that olfactory axons must actively disrupt a basement membrane to enter the brain and suggest alternative putative mechanisms for this, but these are not tested experimentally. In addition, the authors propose that the basement membrane of the olfactory placode acts to resist mechanical forces generated by the morphogenetic movement of the developing brain, and thus to prevent passive deformation of the placode, but this is not tested anywhere, for example by preventing or altering the brain movements in the laminin γ1 mutant.*

We thank the reviewer for the overall positive assessment of our work and for suggesting interesting experiments to attempt in the future, and we carefully responded to all her/his constructive comments below.

> ***Recommendations for the authors:***
>
> ***Reviewer #1 (Recommendations For The Authors):***
>
> *In general, it would be easier to draw conclusions and compare data if the authors used similar stages throughout the article.*

Throughout the article we tried to focus on a series of stages that cover both the coalescence of the OP (up to 24 hpf) and later stages of olfactory system development spanning the brain flexure process (28, 32, 36 hpf). However, for technical reasons it was not always possible to stick to these precise stages in some of our experiments. Also, in Fig. 1E-J, we picked in the movies some images illustrating specific cell or axonal behaviours, and thus the corresponding stages could not match exactly the stage series used in Fig. 1A-D and elsewhere in the article. Nevertheless, this stage heterogeneity does not affect our main conclusions.

> *It would be useful to schematise the olfactory placode and the brain in an insert to clearly visualise the system in each figure.*

We hope that the schematic which was initially presented in Fig. 1K already helps the reader to understand how the system is organised. Although we have not added more schematic views to represent the system in each figure (we think this would make the figures overcrowded), we have added additional legends to point to the OP and the brain in the pictures in order to clarify the localisation of each tissue.

> *In the Summary, the authors refer to the integrity of the basement membrane. I don't think there is any attempt to affect basement membrane integrity in the article. It would be important to do so to look at the effect on CNS-PNS separation and axonal elongation.*

In the Summary, we use the term « integrity of the basement membrane » to mention that we have analysed this integrity in the sly mutant. Given the results of our immunostainings

against three main components of the basement membrane (Laminin, Collagen IV and Nidogen), as well as our EM observations, we see the sly mutant as a condition in which the integrity of the basement membrane is strongly affected.

> *Rescue experiments by locally inducing Laminin expression would have strengthened the paper.*

We have attempted to rescue the sly mutant phenotypes by introducing the mutation in the transgenic *TgBAC(lamC1:lamC1-sfGFP)* background, in which Laminin γ1 tagged with sfGFP is expressed under the control of its own regulatory sequences (Yamaguchi et al., 2022). To do so, we crossed *sly*+/-;*Tg(omp:yfp)* fish with *sly*+/-; *Tg(lamC1:LamC1-sfGFP)* fish. Surprisingly, while a rescue of the global embryo morphology was observed, no clear rescue of the olfactory system defects could be detected at 36 hpf. This could be due to the fact that the expression level of LamC1-sfGFP obtained with one copy of the transgene is not sufficient to rescue the olfactory system phenotypes, or that the sfGFP tag specifically affects the function of the Laminin γ1 chain during the development of the olfactory system, making it unable to rescue the defects. Given the results of our first attemps, we decided not to continue in this direction.

> *(1) Developing OP & brain are surrounded by laminin-containing BM (already described by Torrez-Pas & Whitlock in 2014).*
>
> *"we first noticed the appearance of a continuous Laminin-rich BM surrounding the brain from 14-18 hpf, while around the OP, only discrete Laminin spots were detected at this stage (Fig. 1A, A'). "*
>
> *Around 8ss for Torrez-Pas & Whitlock (before 14 hpf). Can you modify the text, or show an 8ss stage embryo? As far as I know, the authors do not show images at 14hpf. Please correct this sentence or show a 14 hpf picture.*

The reviewer is right, we do not show any 14 hpf stage in the images and thus have removed this stage in the text and replaced it by 17 hpf.

> *In Figure 1A, the labelling of laminin 111 does not appear to be homogeneous along the brain.*
>
> *Is this true?*

At this stage the brain's BM revealed by the Laminin immunostaining appears fairly continuous (while the OP's one is clearly dotty and less defined), but indeed very tiny/local interruptions of the signal can been seen along the structure as detected by the reviewer. We thus modified the text to mention these tiny interruptions.

> *How is the Laminin antibody used by the authors specific to laminin 111?*

We thank the reviewer for raising this important point. The immunogen used to produce this rabbit polyclonal antibody is the Laminin protein isolated from the basement membrane of a mouse Engelbreth Holm-Swarm sarcoma (EHS). It is thus likely to recognise several Laminin isoforms and not only Laminin 111. We thus replaced Laminin 111 by Laminin when mentioning this antibody in the text and Figures.

> *Please schematise in Figure 1K the stages you have tested and shown here in the article i.e. stages 18 - 22 - 28 -36 hpf using immunohistochemistry and 17-26-27-29-33 and 38 hpf using transgenics for laminin 111 and LamC1 respectively.*

As suggested by the reviewer, we changed the stages in the schematics for stages we have presented in Figure 1 (analysed either with immunostaining or in live imaging experiments). We chose to represent 17 - 22 - 26 - 33 hpf (and thus adapted some of the schematics for them to match these stages).

> *Please specify in the Figure 1 legend for panels A to D whether this is a 3D projection or a zsection.*

We indicated in the Figure 1 legend that all these images are single z-sections (as well as for panels E-J).

> *Furthermore, the schematisation in Fig. 1K does not reflect what the authors show: at 22 hpf laminin 111 labelling appears to be present only near the brain, and no labelling lateral to the olfactory placode and anteriorly and posteriorly. Thus, the schematisation in Figure 1K needs to be modified to reflect what the authors show.*

We agree with the reviewer that the Laminin staining at this stage is observed around the medial region of the OP, but not more laterally. We modified the schematic view accordingly in Figure 1K. Anterior and posterior sides of the OP are not represented in this schematic because we chose to represent a frontal view rather than a dorsal view.

> *The authors suggest that" the laminin-rich BM of OP assembles between 18 and 22 hpf, during the late phase of OP coalescence". However, their data indicate that this BM assembles around 28hpf (Figure 1C). Can they clarify this point?*

What we meant with this sentence is that we cleary see two distinct BMs from 22 hpf. However, as noticed by the reviewer, the OP's BM is only present around the medial/basal regions of the OP and does not surround the whole OP tissue at this stage. We modified the text to clarify this point (in particular by mentioning that the OP's BM starts to assemble between 18 and 22 hpf), and replaced the image shown in Figure 1B, B' with a more representative picture (the previous z-section was taken in very dorsal regions of the OP).

> *It would be useful to disrupt these cells that have a cytoplasmic expression of Laminin-sfGFP, to analyse their contribution to BM and OP coalescence.*

Indeed it will be interesting in the future to test specifically the role of the cells expressing cytoplasmic Laminin-sfGFP around and within the OP, as proposed by the reviewer. Laser ablation of these cells could be attempted, but due to their very superficial localisation, close to the skin, we believe these ablations (with the protocol/set-up we currently use in the lab) would impair the skin integrity, preventing us to conclude. We consider that the optimisation of this experiment is out of the scope of the present work.

> *Tg(-2.0ompb:gapYFP)rw032 marks ciliated olfactory sensory neurons (OSNs) (Sato et al., 2005). The authors should mention this.*

Please see our detailed response to the next point below.

> *Points to be clarified:*
>
> *-Tg(-2.0ompb:gapYFP)rw032 marks ciliated olfactory sensory neurons (OSNs) (Sato et al., 2005). The authors should mention this here. Moreover, the authors refer to "OP neurons" throughout the article. In the development of the olfactory organ, two types of neurons have been described in the literature: early EONs (12hpf-26hpf) and later OSNs. Each could have a specific role in the establishment and maintenance of the BM*

> *described by the authors. The authors need to clarify this point as, in Figure 1 for example, they use a marker for Tg(neurog1:GFP) EONs and a marker for ciliated OSNs without distinction. The distinction between EONs and OSNs comes a little late in the text and should be placed higher up.*

As mentioned by the reviewer, according to the initial view of neurogenesis in the OP, OP neurons are born in two waves. A transient population of unipolar, dendrite-less pioneer neurons would differentiate first, in the ventro-medial region of the OP and elongate their axons dorsally out of the placode, along the brain wall. These pioneer axons would then be used as a scaffold by later born OSNs located in the dorso-lateral rosette to outgrow their axons towards the olfactory bulb (Whitlock and Westerfield, 1998).

Another study further characterised OP neurogenesis and showed that the first neurons to differentiate in the OP (the early olfactory neurons or EONs) express the Tg(neurog1:GFP) transgene (Madelaine et al., 2011). As mentioned by the authors in the discussion of this article, neurog1:GFP+ neurons appear much more numerous than the previously described pioneer neurons, and may thus include pioneers but also other neuronal subtypes.

We would like here to share additional, unpublished observations from our lab that further suggest that the situation is more complex than the pioneer/OSN and EON/OSN nomenclatures. First, in many of our live imaging experiments, we can clearly visualise some neurog1:GFP+ unipolar neurons, initially located in a medial position in the OP, which intercalate and contribute to the dorsolateral rosette (where OSNs are proposed to be located) at the end of OP coalescence, from 22-24 hpf. Second, in fixed tissues, we observed that most neurog1:GFP+ neurons located in the rosette at 32 hpf co-express the Tg(omp:meRFP) transgene (Sato et al., 2005). These observations suggest that at least a subpopulation of neurog1:GFP+ neurons could incorporate in the dorsolateral rosette and become ciliated OSNs during development. We can share these results with the reviewer upon request. Further studies are thus needed to clarify and describe the neuronal subpopulations and lineage relationships in the OP, but this detailed investigation is out of the scope and focus of the present study.

An additional complication comes from the fact that, as shown and acknowledged by the authors in Miyasaka et al., 2005, the Tg(omp:meYFP) line (6kb promoter) labels ciliated OSNs in the rosette but also some unipolar, ventral neurons (around 10 neurons at 1 dpf, Miyasaka et al. 2005, Figure 3A, white arrowheads). This was also observed using the 2 kb promoter Tg(omp:meYFP) line (see for instance Miyasaka et al., 2007) and in our study, we can indeed detect these ventro-medial neurons labelled in the Tg(omp:meYFP) line (2 kb promoter), see for instance Figure 1C', D' or Movie 6. It is unclear whether these unipolar omp:meYFPpositive cells are pioneer neurons or EONs expressing the omp:meYFP transgene, or OSN progenitors that would be located basally/ventrally in the OP at these stages.

For all these reasons, we decided to present in the text the current view of neurogenesis in the OP but instead of attributing a definitive identity to the neurons we visualise with the transgenic lines, we prefer to mention them in the manuscript (and in the rest of the response to the reviewers) as neurons expressing neurog1:GFP or omp:meYFP transgenes (or cells/axons/neurons expressing RFP in the *Tg(cldnb:Gal4; UAS:RFP)* background).

What we also changed in the text to be more clear on this point:

- we moved higher up in the text, as suggested by reviewer 1, the description of the current model of neurogenesis in the OP,

- we mentioned that neurog1:GFP+ neurons are more numerous than the initially described pioneer neurons, as discussed in Madelaine et al., 2011,

- we wrote more clearly that the Tg(omp:meYFP) line labels ciliated OSNs but also a subset of unipolar, ventral neurons (Miyasaka et al., 2005), and pointed to these ventral neurons in Figure 1C', D',

- in the initial presentation of the current view of OP neurogenesis we renamed neurog1:GFP+ into EONs to be coherent with Madelaine et al., 2011.

> *- To visualise pioneer axons, the authors should use an EONS marker such as neurog1 because, to my knowledge, OMP only marks OSN axons and not pioneer axons.*

To visualise neurog1:GFP+ axons during OP coalescence, we performed live imaging upon injection of the neurog1:GFP plasmid (Blader et al., 2003) in the *Tg(cldnb:Gal4; UAS:RFP)* background (n = 4 mutants and n = 4 controls from 2 independent experiments). We observed some GFP+ placodal neurons exhibiting retrograde axon extension in both controls and sly mutants. In such experiments it is very difficult to quantify and compare the number of neurons/axons showing specific behaviours between different experimental conditions/genetic background. Indeed, due to the cytoplasmic localisation of GFP, the axons can only be seen in neurons expressing high levels of GFP, and due to the injection the number of such neurons varies a lot in between embryos, even in a given condition. Nevertheless, our qualitative observations reinforce the idea that the basement membrane is not absolutely required for mediolateral movements and retrograde axon extension of neurog1:GFP+ neurons in the OP. We added examples of images extracted from these new live imaging experiments in the revised Fig. S5A, B.

> *- The authors should analyse the presence of laminin in the OP and forebrain in conjunction with neural crest cell dynamics (using a Sox10 transgenic line for example) to refine their entry and exit point hypotheses.*

As described in the answer to the next point, we performed new experiments in which we visualised NCC migration in the Tg(neurog1:GFP) background, which allowed us to analyse the localisation of NCC at the forebrain/OP boundary, in ventral and dorsal positions, both in sly mutant embryos and control siblings.

> *- A dynamic analysis of the distribution of neural crest cells in the sly mutant over time and during OP coalescence would be important.*

The dynamics of zebrafish cranial NCC migration in the vicinity of the OP has been previously analysed using *sox10* reporter lines (Harden et al., 2012, Torres-Paz and Whitlock, 2014, Bryan et al., 2020). To address the point raised by the reviewer, we performed live imaging from 16 to 32 hpf on sly mutants and control siblings carrying the Tg(neurog1:GFP) and Tg(UAS:RFP) transgenes and injected with a sox10(7.2):KalTA4 plasmid (Almeida et al., 2015). This allows the mosaic labelling of cells that express or have expressed sox10 during their development which, in the head region at these stages, represents mostly NCC and their derivatives. 3 independent experiments were carried out (n = 4 mutant embryos in which 8 placodes could be analysed; n = 6 control siblings in which 10 placodes could be analysed). A new movie (Movie 9) has been added to the revised article to show representative examples of control and mutant embryos.

From these new data, we could make the following observations:

- As expected from previous studies (Harden et al., 2012, Torres-Paz and Whitlock, 2014, Bryan et al., 2020), in control embryos a lot of NCC had already migrated to reach the vicinity of the OP when the movies begin at 16 hpf, and were then seen invading mainly the interface between the eye and the OP (10/10 placodes). Surprisingly, in *sly* mutants, a lot of motile NCC

had also reached the OP region at 16 hpf in all the analysed placodes (8/8), and populated the eye/OP interface in 7/8 placodes (10/10 in controls). Counting NCC or tracking individual NCC during the whole duration of the movies was unfortunately too difficult to achieve in these movies, because of the low level of mosaicism (a high number of cells were labelled) and of the high speed of NCC movements (as compared with the 10 min delta t we chose for the movies).

- in some of the control placodes we could detect a few NCC that populated the forebrain/OP interface, either ventrally, close to the exit point of the axons (4/10 placodes), or more dorsally (8/10 placodes). By contrast, in *sly* mutants, NCC were observed in the dorsal region of the brain/OP boundary in only 2/8 placodes, and in the ventral brain/OP frontier in only 2/8 placodes as well. Interestingly, in these 2 last samples, NCC that had initially populated the ventral region of the brain/OP interface were then expelled from the boundary at later stages.

We reported these observations in a new Table that is presented in revised Fig. S6B. In addition, instances of NCC migrating at the eye/OP or forebain/OP interfaces are indicated with arrowheads on Movie 9. Previous Figure S6 was splitted into two parts presenting NCC defects in *sly* mutants (revised Figure S6) and in *foxd3* mutants (revised Figure S7).

Altogether, these new data suggest that the first postero-anterior phase of NCC migration towards the OP, as well as their migration in between the eye and OP tissues, is not fully perturbed in *sly* mutants. The subset of NCC that populate the OP/forebrain seem to be more specifically affected, as these NCC show defects in their migration to the interface or the maintenance of their position at the interface. Since the *crestin* marker labels mostly NCC at the OP/forebrain interface at 32 hpf (revised Fig. S6A), this could explain why the *crestin* ISH signal is almost lost in *sly* mutants at this stage.

> *(2) Laminin distribution suggests a role in olfactory axon development*
>
> *"Laminin 111 immunostaining revealed local disruptions in the membrane enveloping the OP and brain, precisely where YFP+ axons exit the OP (exit point) and enter the brain (entry point) (Fig. 1C-D')." Can the authors quantify this situation? It would be important to analyse this behaviour on the scale of a neuron and thus axonal migration to strengthen the hypotheses.*

As suggested by the reviewer, to better visualise individual axons at the exit and entry point, we used mosaic red labelling of OP axons. To achieve this sparse labelling, we took advantage of the mosaic expression of a red fluorescent membrane protein observed in the *Tg(cldnb:Gal4; UAS:lyn-TagRFP)* background. The unpublished *Tg(UAS:lyn-TagRFP)* line was kindly provided by Marion Rosello and Shahad Albadri from the lab of Filippo Del Bene. We crossed the *Tg(cldnb:Gal4; UAS:lyn-TagRFP)* line with the *TgBAC(lamC1:lamC1-sfGFP)* reporter and performed live imaging on 2 embryos/4 placodes, in a frontal view. A new movie (Movie 3 in the revised article) shows examples of exit and entry point formation in this context.This allowed us to visualise the formation of the exit and entry points in more samples (6 embryos and 12 placodes in total when we pool the two strategies for labelling OP axons) and through the visualisation of a small number of axons, and reinforce our initial conclusions.

> *(3) The integrity of BMs around the brain and the OP is affected in the sly mutant*
>
> *Why do the authors analyse the distribution of collagen IV and Nidogen and not proteoglycans and heparan sulphate?*

We attempted to label more ECM components such as proteoglycans and heparan sulfate, but whole-mount immunostainings did not work in our hands.

> *A dynamic analysis of the distribution of neural crest cells in the sly mutant over time and during OP coalescence would be important.*

See our detailed response to this point above.

> *(4) Role of Laminin γ1-dependent BMs in OP coalescence*
>
> *The authors use the size of the Tg(neurog1:GFP)+ OP cell cluster at 22 hpf as a marker. The authors should count the number of cells in the OP at the indicated time using a nuclear dye to check that in the sly mutant the number of cells is the same over time. Two time points as analysed in Figure S2 may not be sufficient to quantify proliferation which at these stages should be almost zero according to Whitlock & Westerfield and Madelaine et al.*

Counting the neurog1:GFP+ cell numbers in our existing data was unfortunately impossible, due to the poor quality of the DAPI staining. We are nevertheless confident that the number of cells within neurog1:GFP+ clusters is fairly similar between controls and sly mutants at 22 hpf, since the OP dimensions are the same for AP and DV dimensions, and only slightly different for the ML dimension. In addition, we analysed proliferation and apoptosis within the neurog1:GFP+ cluster at 16 and 21 hpf and observed no difference between controls and mutants.

> *(5) Role of Laminin γ1-dependent BMs during the forebrain flexure*
>
> *In Figure 4F at 32hpf, the presence of 77% ectopic OMP+ cells medially should result in an increase in dimensions along the M-L? This is not the case in the article. The authors should clarify this point.*

As we explained in the Material and Methods, ectopic fluorescent cells (cells that are physically separated from the main cluster) were not taken into account for the measurement of the OP dimensions. This is now also also mentioned in the legends of the Figures (4 and S3) showing the quantifications of OP dimensions.

> *Cell distribution also seems to be affected within the OMP+ cluster at 36hpf, with fewer cells laterally and more medially. The authors should analyse the distribution of OMP+ cells in the clusters. in sly mutants and controls to understand whether the modification corresponds to the absence of BM function.*

On the pictures shown in Figure 4F,G, we agree that omp:meYFP+ cells appear to be more medially distributed in the mutant, however this is not the case in other sections or samples, and is rather specific to the z-section chosen for the Figure. We found that the ML dimension is unchanged in mutants as compared with controls, except for the 28 hpf stage where it is smaller, but this appears to be a transient phenomenon, since no change is detected at earlier or later stages (Figure 4A-D and Figure S3A-L). The difference we observe at 28 hpf is now mentioned in the revised manuscript.

> *The conclusions of Figures 4 and S3 would rather be that laminin allows OMP+ cells to be oriented along the medio-lateral axis whereas it would control their position along the dorsoventral axis. The authors should modify the text. It would be useful to map the distribution of OMP+ cells along the dorsoventral and mediolateral axes. The same applies to Neurog1+ cells. An analysis of skin cell movements, for example, would be useful to determine whether the effects are specific.*

We are confident that the measurements of OP dimensions in AP, DV and ML are sufficient to describe the OP shape defects observed in the sly mutants. Analysing cell distribution along the 3 axes as well as skin cell movements will be interesting to perform in the future but we consider these quantifications as being out of the scope of the present work.

> *(6) Laminin γ1-dependent BMs are required to define a robust boundary between the OP and the brain*
>
> *The authors must weigh this conclusion "Laminin γ1-dependent BMs serve to establish a straight boundary between the brain and OP, preventing local mixing and late convergence of the two OPs towards each other during flexion movement." Indeed, they don't really show any local mixing between the brain and OP cells. They would need to quantify in their images (Figure 5A-A' and Figure S4 A-A') the percentage of cells co-labelled by HuC and Tg(cldnb:GFP).*

We agree with the reviewer and thus replaced « reveal » by « suggest » in the conclusion of this section.

> *(7) Role of Laminin γ1-dependent BMs in olfactory axon development*
>
> *An analysis of the retrograde extension movement in the axons of OMP+ ectopic neurons in the sly1 mutant condition would be useful to validate that the loss of laminin function does not play a role in this event.*

Indeed, even though we can visualise instances of retrograde extension occurring normally in *sly* mutants, we can not rule out that this process is affected in a subset of OP neurons, for instance in ectopic cells, which often show no axon or a misoriented axon. We added a sentence to mention this in the revised manuscript.

> *Minor comments and typos:*
>
> *Please check and mention the D-V/L-M or A-P/L-M orientation of the images in all figures.*

This has been checked.

> *Legend Figure 1: "distalmost" is missing a space "distal most".*

We checked and this word can be written without a space.

> *Figure 1 panel C: check the orientation (I am not sure that Dorsal is up).*

We double-checked and confirm that dorsal is up in this panel.

> *Movie 1 Legend: "aroung "the OP should be around the OP.*

Thanks to the reviewer for noticing the typo, we corrected it.

> ***Reviewer #2 (Recommendations For The Authors):***
>
> *The comments below are relatively minor and mostly raise questions regarding images and their presentation in the manuscript.*
>
> *• Figure 1, visualization of exit and entry points: It is a bit difficult to visualize the axon exit and entry points in these images, and in particular, to understand how the exit and entry points in C and D correspond to what is seen in F, F', H, and H'. There appears to be*

> *one resolvable break in the staining in C and D, whereas there are two distinct breaks in F-H'. Are these single optical sections? Is it possible to visualize these via 3-dimensional rendering?*

All the images presented in Figure 1 are single z-sections, which is now indicated in the Figure legend. As noticed by the reviewer, Laminin immunostainings on fixed embryos at 28 and 36 hpf suggested that the exit and entry points are facing each other, as shown in Figure 1C-D'. However, in our live imaging experiments we always observed that the exit point is slightly more ventral than the entry point (of about 10 to 20 µm). This discrepancy could be due to the fixation that precedes the immunostaining procedure, which could modify slightly the size and shape of cells/tissues. We added a sentence on this point in the text. In addition, we added new movies of the *LamC1-sfGFP* reporter with sparse red axonal labelling (Movie 3, see response to reviewer 1), as well as z-stacks presenting the organisation of exit and entry points in 3D (Movie 4), which should help to better illustrate the mechanisms of exit and entry point formation.

> *• Movie 2, p. 6, "small interruptions of the BM were already present near the axon tips, along the ventro-medial wall of the OP." This is a bit difficult to assess since the movie seems to show at least one other small interruption in the BM in addition to the exit point, in particular, one slightly dorsal to the exit point. Was this seen in other samples, or in different optical sections?*

Indeed the exit and entry points often appear as regions with several, small BM interruptions, rather than single holes in the BM. We now show in revised Movie 4 the two z-stacks (the merge and the single channel for green fluorescence) corresponding to the last time points of the movies showing exit and entry point formation in Movie 2, where several BM interruptions can be seen for both the exit and entry points. We had already mentioned this observation in the legend of Movie 2, and we added a sentence on this point in the main text of the revised manuscript. This is also represented for both exit and entry points in the new schematics in revised Fig. 1K and its legend.

> *• Movie 2, p. 6, "The opening of the entry point through the brain BM was concomitant with the arrival of the RFP+ axons, suggesting that the axons degrade or displace BM components to enter the brain." Similar to the questions regarding the exit point, it was a bit difficult to evaluate this statement. There appears to be a broader region of BM discontinuity more dorsal to the arrowhead in Movie 2. A single-channel movie of just the laminin fluorescence might help to convey the extent of the discontinuity. As with above, was this seen in other samples, or in different optical sections?*

See our response to the previous comment.

> *• Figure 1H, I, "the distal tip of the RFP+ axons migrated in close proximity with the brain's BM." This is again a bit difficult to see, and quite different than what is seen in Figure 4A, in which the axons do not seem close to the BM in this section. Is it possible to visualize this via 3-dimensional rendering?*

In fixed embryos or in live imaging experiments, we observed that, once entered in the brain, the distal tips (the growth cones) of the axons are located close to the BM of the brain. However, this is not the case of the axon shafts which, as development proceeds, are located further away from the BM. This can clearly be seen at 36 hpf in Figure 1D' and Figure 4A, as spotted by the reviewer. We modified the text to clarify this point.

> *• Figure 2J, J', p. 7, the gap between the OP and brain cells of sly mutants "was most often devoid of electron-dense material." It is difficult to see this loss of electron-dense material*

> *in 2J'. The thickness of the space is quantified well and is clearly smaller, but the change in electron-dense material is more difficult to see.*

We looked at Figure 2 again and it seems clear to us that there is electron-dense material between the plasma membranes in controls, which is practically not seen (rare spots) in the mutants. We added a sentence mentioning that we rarely see electron-dense spots in sly mutants.

> *• Figure 5E-F': There are concerns about evaluating the shape of a tissue based on nuclear position. Is there a way to co-stain for cell boundaries (maybe actin?), and then quantify distortion of the dlx+ cell population using the cell boundaries, rather than nuclear staining?*

We agree with the reviewer that it is not ideal to evaluate the shape of the OP/brain boundary based on a nuclear staining. As explained in the text, we could not use the *Tg(eltC:GFP)* or *Tg(cldnb:Gal4; UAS:RFP)* reporter lines for this analysis, due to ectopic or mosaic expression. However we are confident that the segmentation of the Dlx3b immunostaining reflects the organisation of the cells at the OP/brain tissue boundary: in other data sets in which we performed Dlx3b staining with membrane labelling independently of the present study and in the wild type context, we clearly see that cell membranes are juxtaposed to the Dlx3b nuclear staining (in other words, the cytoplasm volume of OP cells is very small).

> *• Figure S5E: It would be helpful to see representative images for each of the categories (Proper axon bundle; Ventral projections; Medial projections) or a schematic to understand how the phenotypes were assessed.*

To address this point we added a schematic view to illustrate the phenotypes assessed in each column of the table in revised Figure S5G.

> *• Figure 6, p. 12, "Laminin gamma 1-dependent BMs are essential for growth and navigation of the axons...": What fraction of the tracked axons managed to exit the OP? Given the quantitative analyses in Figure 6, one might interpret this to mean that laminin gamma 1 is not essential for axon growth (speed and persistence are largely unchanged), but rather, primarily for navigation.*

As noticed by the reviewer, the speed and persistence of axonal growth cones are largely unchanged in the sly mutants (except for the reduced persistence in the 200-400 min window, and an increased speed in the 800-1000 min window), showing that the growth cones are still motile. However, as shown by the tracks, they tend to wander around within the OP, close to the cell bodies, which results in the end in a perturbed growth of the axons. The navigation issues are rather revealed by the analysis of fixed Tg(omp:meYFP) embryos presented in the table of Figure S5G. We modified the text to separate more clearly the conclusions of the two types of experiments (fixed, transgenic embryos versus live, mosaically labelled embryos).

> ***Reviewer #3 (Recommendations For The Authors):***
>
> *Testing the hypotheses mentioned in the public review will be interesting experiments for a follow-up study, but are not essential revisions for this manuscript.*
>
> *I have only a few minor suggestions for revisions:*
>
> *P8 subheading 'Role of Laminin γ1-dependent BMs in OP coalescence' - since no major role was demonstrated here, this heading should be reworded.*

We agree with the reviewer and replaced the previous title by « OP coalescence still occurs in the *sly* mutant ».

> *P11, line 3 - the authors conclude that the forebrain is smaller 'due to' the inward convergence of the OPs. I do not think it is possible to assign causation to this when the mutant disrupts Laminin y1 systemically - it is equally possible that the OPs move inward due to a failure of the brain to form in the normal shape. Thus, the wording should be changed here. (In the Discussion on p15, the authors mention the 'apparent distortion' of the brain, and say that it is 'possibly due' to the inward migration of the placodes', but again this could be toned down.)*

We agree with the reviewer's comment and changed the wording of our conclusions in the Results section.

> *P11 and Fig. S5 - The table and text seem to be saying opposite things here. The text on p11 (3rd paragraph) indicates that the normal exit point is ventral and that this is disrupted in the mutant, with axons exiting dorsally. However, in the table, at each time point there is a higher % of axons exiting ventrally in the mutant. Please clarify. The table does not provide a % value for axons exiting dorsally - it might help to add a column to show this value.*

We are grateful to the reviewer for pointing this out, and we apologize for the lack of clarity in the first version of the manuscript. We have modified the text and Figure S5 in order to clarify the different points raised by the reviewer in this comment. The Table in Fig. S5G does not represent the % of axons showing defects, but the % of embryos showing the phenotypes. In addition, an embryo is counted in the ventral or medial projection category if it shows at least one ventral or medial projection (even if its shows a proper bundle). This is now clearly indicated in the title of the columns in the table itself and in the legend. The embryos in which the axons exit dorsally in sly mutants are actually those counted in the left column of the Table (they exit dorsally and form a bundle), as shown by the new schematics added below the table. We also added this information in the title of the left column, and mention in the legend the pictures in which this dorsal exit can be observed in the article (Figures 4B and S3E'). Having more sly mutant embryos with axons exiting dorsally is thus compatible with more embryos showing at least one ventral projection.

> *Fig. S6, shows the lack of neural crest cells between the olfactory placode and the brain in both laminin y1 mutants (without a basement membrane) and foxd3 mutants (which retain the membrane). Comparison of the two mutants here is a neat experiment and the result is striking, demonstrating that it is the basement membrane, and not the neural crest, that is required for correct morphology of the olfactory placode. I think this figure should be presented as a main figure, rather than supplementary.*

Our new live imaging characterisation of NCC migration in sly mutants and control siblings (Movie 9) revealed that at 32 hpf, in the vicinity of the OP, NCC (or their derivatives) are much more numerous than the subset of NCC showing crestin expression by in situ hybridisation (compare the end of our control movie – 32 hfp, with crestin ISH shown in Figure S6A for instance).

Thus, the extent of the NCC migration defects should be analysed in more detail in the foxd3 mutant in the future (using live imaging or other NCC markers), and for this reason we chose to keep this dataset in the supplementary Figures.

> *One of the first topics covered in the Discussion section is the potential role of Collagen. I was surprised to see the description on P15 'the dramatic disorganization of the Collagen*

> *IV pattern observed by immunofluorescence in the sly mutant', as I hadn't picked this up from the Results section of the paper. I went back to the relevant figure (Fig. 2) and description on p7, which does not give the same impression: 'in sly mutants, Collagen IV immunoreactivity was not totally abolished'. This suggested to me that there was only minor (not dramatic) disorganisation of the Collagen IV. This needs clarification.*

The linear, BM-like Collagen IV staining was lost in sly mutants, but not the fibrous staining which remained in the form of discrete patches surrounding the OP. We modified the text in the Results section as well as in the Figure 2 legend to clarify our observations made on embryos immunostained for Collagen IV.

> *Typos etc*
>
> *P5 - '(ii) above of the neuronal rosette' - delete the word 'of'.*
>
> *P5 two lines below this - ensheathed.*
>
> *P10 - '3 distinct AP levels' (delete s from distincts).*
>
> *P10 - distortion (not distorsion) .*
>
> *P12 - 'From 14 hpf, they' should read 'From 14 hpf, neural crest cells'.*
>
> *P15, line 1 - 'is a consequence of' rather than 'is consecutive of'?*
>
> *P22 'When the data were not normal,' should read 'When the data were not normally distributed,'.*

We thank the reviewer for noticing these typos and have corrected them.

> *General*
>
> *Please number lines in future manuscripts for ease of reference.*

This has been done.

https://doi.org/10.7554/eLife.92004.2.sa0